scientific reports

Check for updates

OPEN

Mesoporous magnetic supported Cu complex for one-pot synthesis of 5-substituted 1*H*-tetrazoles in green media and the oxidation of sulfides

Somayeh Molaei & Mohammad Ghadermazi✉

We used the copper Phthalocyanine (Pc) on magnetic mesoporous silica nanoparticles. Therefore, several coordination sites became available which enhance chelating potency to load appropriate amounts of Gadolinium (Gd). This improves the catalytic activity in converting nitrile to tetrazole and selective oxidation of sulfides. Gadolinium (Gd) with incompletely occupied 4*f* and empty 5*d* orbitals can be used as the active component or as the promoter of the catalyst. Here, we outline the synthesis, characterization, and catalytic activity of a novel Gd(III) copper Phthalocyanine (Pc) coordination on the $CoFe_2O_4$/SBA-15 ($CoFe_2O_4$/SBA-15/CuPc@Gd). The prepared material was characterized using powder X-ray diffraction, field emission scanning electron microscopy, transmission electron microscopy, elemental mapping, vibrating-sample magnetometer (VSM), Inductively coupled plasma atomic emission spectroscopy (ICP-AES), Fourier transform infrared spectroscopy, and nitrogen adsorption–desorption isotherm. The $CoFe_2O_4$/SBA-15/CuPc@Gd composite consists of a mesoporous structure with a surface area by BET and t-plot of 122.2 m^2/g and 86.28 m^2/g respectively, with a mean pore size of 5.37 nm, and pore volume of 0.164 cm^3/g. The $CoFe_2O_4$/SBA-15/CuPc@Gd was successfully applied as a powerful catalyst for green synthesis of 5-substituted 1*H*-tetrazoles in water and selective oxidation of sulfides at room temperature. This catalyst was recovered and reused several times without a significant decrease in efficiency and stability. The catalyst could be fully recovered by an external magnetic field and showed good reusability.

Phthalocyanines (Pcs) have been used in solar cells, sensors, semiconductors, photodynamic treatment (PDT), catalysis, coloring dyes for clothes and plastics, and several applications[1–4]. These macrocycles, comprised of four isoindole units connected by aza bridges, also feature a rich metalation chemistry that allows several metal ions in their core. These ions vary in size and charge, directly affecting the macrocycles' photochemical and photophysical properties allowing customization based on the application[5]. Under mild conditions, MPcs are considered effective catalysts for the oxidation of hydrocarbons, phenols, alcohols, and other organic molecules as well as the degradation of contaminants[6–8]. Pcs have superior performance over porphyrins in some cases, making them a great option for artificial biomimetic catalysts. Compared to porphyrin derivatives, the Pc-based catalysts have additional benefits that are generally associated with their structural, chemical, and thermal stability, cost-effectiveness, and capacity for large-scale manufacturing. However, Pcs' strong aggregation tendency and lack of solubility in common solvents make them unsuitable as catalysts in homogenous environments. Moreover, under typical catalytic circumstances, homogeneous catalysts based on Pcs tend to break down because of Pc auto-oxidation, which makes it difficult for these compounds to be recovered and reused[3]. Several methods to immobilize the core catalysts (Pcs) have already been researched and developed to solve these issues[7,9–11].

One of the important approaches of green chemistry is the use of recyclable catalysts[12,13]. Although homogeneous catalysts have many advantages such as high efficiency and selectivity, but from the point of

Department of Chemistry, Faculty of Science, University of Kurdistan, Sanandaj, Iran. ✉email: mghadermazi@yahoo.com

view of green chemistry, there are drawbacks in the separation and recycling of catalysts from the product such as tedious and time-consuming work-up procedures. This problem is a big challenge especially when the expensive catalyst is used in large quantities[14–16]. A great deal of attention has been paid to develop methods for heterogenizing homogeneous catalysts to combine the advantages of both homogeneous and heterogeneous catalysis[17]. The immobilization of homogeneous catalysts on a large variety of organic or inorganic supports such as silica materials, zeolites, organosilica materials, aluminas, magnetic nanoparticles, polymers, biochar, and carbon materials to create heterogeneous catalysts is an effective strategy that has been developed in recent years[18–25].

Many distinct mesoporous materials with large volume, pore size, and surface area have already been synthesized using various surfactant templating strategies. These materials' unique functional applications in the field of heterogeneous organic catalysts are developed by utilizing the immobilization of organic functional groups[26–30]. Over the past ten years, many researches have been done on customized mesoporous materials with lots of active sites[31]. Among various supports, mesoporous silica materials, because of their various advantages such as high surface area, tunable pore size, nanometer sized pore, great chemical and mechanical stability, and controlled size have attracted much attention[14]. Customizing the surface area properties of mesoporous silica through organo-functional modification is advantageous for several applications within the realm of heterogeneous catalysis[32–34]. Li et al. used the three siliceous materials as VPO supports for both n-butane and propane partial oxidation. The $(VO)_2P_2O_7$ have been successfully supported onto SBA-15, MCM-41, and fumed SiO_2. As revealed by XPS and small-angle XRD results, the highest VPO dispersion was observed over the SBA-15 sample, while the lowest VPO dispersion was observed over the nonporous fumed SiO_2 sample[35]. The siliceous support SBA-15 has thermal stability, wide surface area, large pore volume, and uniform pore-size distributions, which makes it an appropriate choice for the binding of organo-catalysts[36–38]. Furthermore, SBA-15 is a promising porous solid due to its capacity to host a wide range of functional groups through co-condensation, isomorphic replacement, or grafting[39]. This presents a highly valuable opportunity to develop solids with very specific characteristics for use in pharmaceutical applications such as drug delivery, biosensing, and catalysis, as well as industrial applications related to adsorption processes and membrane separation[40–44]. To develop effective heterogeneous catalysts, magnetically responsive systems are an excellent alternative to catalyst systems. However, filtration or centrifugation are tedious and time-consuming methods of separating these particles from the reaction mixture. Magnetic nanoparticles (MNPs), which are easily separated from the reaction medium by applying an external magnetic field, could be used to solve this problem. In fact, the integration of magnetic nanoparticles with mesoporous silica nanoparticles generated a novel support that possesses the features and benefits of both mesoporous silica and magnetic nanoparticles[14].

Due to their environmental compatibility, stability, and ease of synthesis, spinel ferrites, MFe_2O_4 (M = Fe, Mn, Co, Ni, Cu, Zn), have recently attracted significant attention in the fields of magnetic resonance imaging, controlled drug release, superparamagnetic materials, electrocatalytic energy conversion, biosensing, and organic pollutant degradation[45–51]. Due in large part to their synergistic intermetallic contacts and magnetic recovery capabilities, they have been employed extensively as heterogeneous catalysts in numerous organic processes[52,53]. $CoFe_2O_4$ nanoparticles have a broad range of uses in drug delivery, magnetic storage, and magnetic response imaging due to their high saturation magnetization, specific surface areas, and coercivity[54–57].

Tetrazole is one of the heterocyclic compounds that consists of a five-membered ring and contains four nitrogen atoms and one carbon atom[58,59]. Tetrazoles have important features due to their many uses in various industrial and synthetic processes[60–62]. Among the drug compounds containing tetrazole ring, we can mention antibacterial drug, antimicrobial, antiviral, antidiabetic, antischizophrenic, antihypertensive drug, and cyclooxygenase-2 inhibitor[63–67]. Also, tetrazoles have applications as ligands in coordination chemistry and catalysis technology, as stable surrogates for carboxylic acids in medicinal chemistry, as effective stabilizers of metallopeptide structures in organometallic chemistry, etc.[15,68–71]. The synthesis of tetrazole ring is a vital step in organic and medicinal chemistry, and various methods have been provided for the synthesis of these compounds[16,25,67,70].

Sulfur compounds are one of the main sources of environmental pollution. Removing sulfur from petroleum compounds is a very important part of modern refining. Oxidation reactions are one of the simple and efficient methods for the transformation of organic functional groups[61,72]. This method selectively oxidizes sulfur-containing organic compounds to sulfoxide or sulfone. Sulfoxide derivatives are an important material in organic chemistry[73,74]. Also, sulfoxide derivatives have some biological activities such as antiulcer, antibacterial, antifungal, antiatherosclerotic, and anti-hypertensive[75–78].

Many homogeneous and heterogeneous catalysts were used to prepare tetrazoles, the results of some conversion of nitrile to tetrazole based on copper, boehmite, non-magnetic, magnetic, MCM-41, carbon, and ZnO nanoparticle catalysts are summarized in Table 1. Although many of these catalysts are efficient in the synthesis of tetrazole derivatives, many of them have one or more of the following difficulties: use of organic solvents, long times, high temperature, non-reusability of the homogeneous catalyst, low tetrazole yields, toxic reaction conditions, formation of side product such as stable metal-tetrazole complexes and tiresome workup of the reaction mixture. Therefore, it is highly desirable to progress an efficient catalyst for the selective synthesis of tetrazole under mild reaction conditions in a benign environmental solvent. The $CoFe_2O_4$/SBA-15/CuPc@Gd exhibits better reaction time, and recyclability under mild conditions.

Rare earth elements having incompletely occupied 4f and unoccupied 5d orbitals can be employed as an active component or a catalytic promoter[79,80]. Meng et al. recently showed that adding an appropriate amount of samarium (Sm) to MnO_x (Sm/Mn = 0.1) can improve the low-temperature performance of MnO_x as well as the stability against water vapor and sulfur toxicity[81]. Sun et al. discovered that adding europium (Eu) to MnOx improves SCR performance and resistance to water vapor and sulfur toxicity, as well as broadening the working temperature window[82], Similarly, Zhu et al. found that doping holmium (Ho) improved the catalytic activity

Entry	Catalyst	Catalyst loading (mg or mol%)	T (°C)	Solvent	Time (h)	Yield (%)	References
1	Boehmite@SiO$_2$@Tris-Cu(I)	0.2 mol%	120	PEG (Poly (ethylene glycol)-400	120	89	[91,92]
2	BNPs@Cur-Ni	40 mg	120	PEG-400	75 min	97	[91,93]
3	Cu-Guanidine@BO-NPs	40 mg	120	PEG-400	70 min	95	[91,94]
4	Pd-SMTU @boehmite	20 mg	120	PEG-400	2.5	95	[91,95]
5	Pd-Arg@boehmite	25 mg	120	PEG-400	7	97	[91,96]
6	Pd-isatin@boehmite	35 mg	120	PEG-400	7	96	[97]
7	CoFe$_2$O$_4$@glycine-Yb	70 mg	120	PEG-400	2.33	93	[98]
8	Methionine@Fe$_3$O$_4$	50 mg	120	DMSO	0.166	100	[99]
9	Fe$_3$O$_4$@SiO$_2$-APTES-TFA	100 mg	80	Ethanol	4	97	[100]
10	Cu-TBA@biochar	0.78 mol%	130	PEG	7	98	[101]
11	SBA-15@glycine-Cu	40 mg	100	PEG	110 min	98	[102]
12	Cu (II)-DCC-CMK-3	20 mg	120	PEG	90 min	97	[103]
13	Cu-MOFs-2 (Cu-TMU-17-NH$_2$)	50 mg	110	PEG	5	95	[104]
14	SO$_3$H@MCM-41	50 mg	80	DMF	1.6	90	[105]
15	Pd-SBT@MCM-41	35 mg	120	PEG-400	6.75	97	[106]
16	L-Cysteine@MCM-41	2.9 mol%	100	PEG-400	2.5	97	[107]
17	Ni-cytosine@MCM-41	0.1 mol%	120	PEG-400	1	92	[108]
18	Fe$_3$O$_4$@MCM-41-SB-Cu	30 mg	120	DMF	1	95	[14]
Entry	Carbon-based nano-catalyst	Catalyst loading (mg or mol%)	T (°C)	Solvent	Time (h)	Yield (%)	References
19	ZrFe$_2$O$_4$@SiO$_2$–N–(TMSP)–ASP–Pd$^{(0}$	15 mg	120	PEG-400	8	97	[109]
20	[Fe$_3$O$_4$@TAM-Schiff-base Cu (II)]	25 mg	120	PEG-400	100	98	[110]
21	Fe$_3$O$_4$-CNT-TEA-Cu (II)	5 mg	70	DMF	1.50	96	[111]
22	GO/Fe$_3$O$_4$@PAA-Cu-complex	20 mg	100	PEG-400	7	98	[112]
23	ZnO	100 mg	120–130	DMF	14	69–82	[113]
24	ZnO/Co$_3$O$_4$	50 mg	120	DMF	12	90	[114]
25	MnCl$_2$.4H$_2$O	10 mol %	120	DMSO	1	92	[115]
26	Pd/AlO(OH) NP	30 mg	78	EtOH	4	73	[116]
27	Fe$_3$O$_4$@MCM-41@Cu-P2C	20 mg	120	PEG	3.5	95	[117]
28	CoFe$_2$O$_4$/SBA-15/CuPc@Gd	100 mg	Boiling point	H$_2$O	60 min	65	This Work

Table 1. Catalytic performance of different catalysts for the synthesis of 5-substituted-1H-tetrazole via a [3 + 2] cycloaddition reaction.

of the Fe–Mn/TiO$_2$ catalyst[83]. These successful studies confirm that rare earth elements can be used to boost the catalyst. Gadolinium (Gd) is a lanthanide situated in the middle of the periodic table that has been used in different fields, mainly for magnetic resonance imaging contrast agents, due to the unusual magnetic properties of the Gd(III) ion[84]. In detail, the Gd(III) has seven unpaired electrons on each orbit which can give rise to large magnetic moments[84]. In addition, Gd as dopant can also be conductive in improving the photocatalytic performances of TiO$_2$, MoO$_3$, and Bi$_2$MoO$_6$[85–88], the dry reforming of methane for Ni/ZSM-5 catalysts[89], and the ethanol oxidation and ethylene production of Cr$_2$O$_3$[90].

One of the important approaches in green chemistry is the tendency to development of recyclable catalysts. Another principle of green chemistry is the use of green solvents and the replacement of highly toxic and volatile organic solvent. We used copper Phthalocyanine (Pc) on magnetic mesoporous silica nanoparticles. Therefore, several good coordination sites are available that enhance chelating potency to load appropriate amounts of Gadolinium (Gd) and therefore improve catalytic activity in converting nitrile to tetrazole and selective oxidation of sulfides. Gadolinium has rarely been reported as a catalyst for the synthesis of organic compounds. This is the first time for reactions of CoFe$_2$O$_4$/SBA-15 supported copper Phthalocyanine (Pc), with Gd salts. For effective synthesis of tetrazole and selective oxidation of sulfides. The reactions are based on green chemistry under mild reaction conditions in green solvent. At a relatively low temperature compared to the reported work, tetrazole derivatives are prepared in water solvent with good efficiency.

Material and methods
Preparation of the CoFe$_2$O$_4$ nanoparticles
To produce CoFe$_2$O$_4$ nanoparticles using the coprecipitation method, 50 mL of distilled water was used to dissolve 0.5 mmol of CoCl$_2$·2H$_2$O powder and 1 mmol of FeCl$_3$·6H$_2$O powder. while being gassed with nitrogen. The first solution was then gradually supplemented with 25 mL dissolved NaOH (1 g. 25 mmol). For three hours, the final solution was refluxed. Following the reaction's cooling to room temperature, the black precipitate that

had formed was separated using a magnet. The resulting $CoFe_2O_4$ nanoparticles were subsequently washed with ethanol and dried at 61 °C[118].

Preparation of the SBA-15

First, 30 mL of H_2O and 90 mL of HCl (2 M) were combined with 4.0 g (0.7 mmol) of Pluronic P123, then the mixture was agitated at 30 °C for 5 h. Subsequently, after gradually adding tetraethylorthosilicate (9.04 mL, 40 mmol), the mixture was agitated for 20 h. After being separated, the outcome was washed, dried, and stored. The sample then received a 5-h calcination at 823 K[119].

Preparation of the CoFe₂O₄/SBA-15

Using the wet impregnation approach, 2.0 g (8.5 mmol) of $CoFe_2O_4$ nanoparticles were added to a mixture of ethanol and deionized water (1:1). Following a 20-min sonication process to disperse the solution, 1.72 g (28.7 mmol) of SBA-15 and 5 mL of aqueous ammonia were added. The mixture was stirred for a further 24 h at room temperature. Following their separation using an external magnet, they were rinsed using deionized water and ethanol, the resulting $CoFe_2O_4$/SBA-15 nanocomposite was dried for 12 h at 80 °C.

Preparation of the CoFe₂O₄/SBA-15/CuPc@Gd

30 mL of DMF was used to dispersion of 30 mg of $CoFe_2O_4$ /SBA-15, and subjected to a 1-h sonication. Subsequently, a solution of 10 mg (17.3 mmol) of copper(II) phthalocyanine in dimethyl formamide (DMF) was added. One more thirty minutes were spent sonicating the solution and then it was stirred continuously for another 24 h. Following that, finally, the dark samples were centrifuged, and the solid was washed three times with DMF and twice with ethanol before being dried for 12 h at 80 °C. After that, 1 g $CoFe_2O_4$/SBA-15/CuPc with 30 mL of ethanol solvent and 2 mmol of Gd $(NO_3)_3$ were combined, and the reaction mixture was refluxed for 24 h (Fig. 1).

Spectral data

5-(3-Nitrophenyl)-1*H*-tetrazole
(Table 4, Entry1): ^{1}HNMR (400 MHz, DMSO, ppm): δ 8.88 (s, 1H), 8.48–8.51 (m, 2H), 7.90–7.97 (m, 1H).
5-(4-Nitrophenyl)-1*H*-tetrazole
(Table 4, Entry 2): ^{1}HNMR (400 MHz, DMSO, ppm): δ 8.50–8.53 (d, 2H), 8.40–8.44 (d, 2H).
5-(4-Bromophenyl))-1*H*-tetrazole
(Table 4, Entry 4): ^{1}HNMR (400 MHz, DMSO, ppm): δ 7.87–7.89 (m, 4H).
Methyl phenyl sulfoxide
(Table 6, Entry 1): ^{1}HNMR (400 MHz, CDCl₃, ppm): δ 2.98 (s, 3H), 7.46– 7.48 (m, 2H), 7.55–7.59 (m, 1H), 7.85–7.87 (m, 2H).
Dibenzyl Sulfoxide
(Table 6, Entry 5): ^{1}HNMR (400 MHz, CDCl₃, ppm): δ 4.16 (s, 4H), 7.40–7. 45 (m, 10H). Benzyl phenyl sulfoxide
(Table 6, Entry 7): ^{1}HNMR (400 MHz, DMSO, ppm): δ 4.68 (s, 2H), 7.14–7.16 (m, 2H), 7.28–7.34 (m, 3H) 7.53–7.62 (m, 2H) 7.71–7.75 (m, 3H).
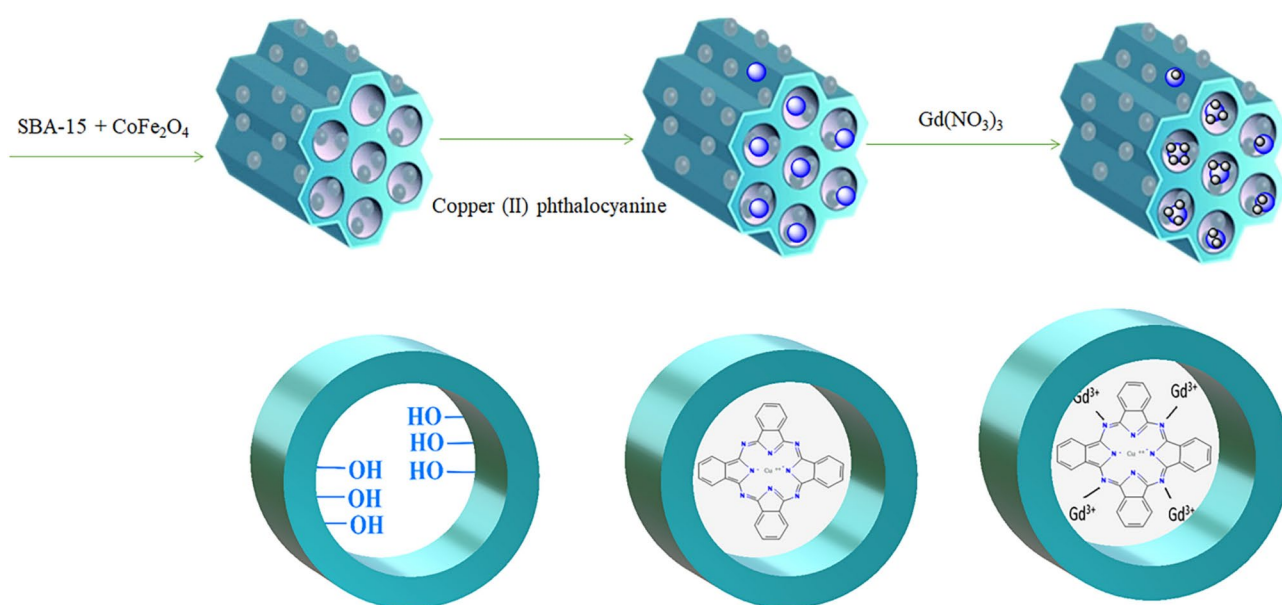

Fig. 1. Diagrammatic representation of the synthesis of the $CoFe_2O_4$/SBA-15/CuPc@Gd.

Results and discussion
Catalyst characterization
XRD analysis

The XRD patterns for the $CoFe_2O_4$/SBA-15 and $CoFe_2O_4$/SBA-15/CuPc@Gd catalysts are shown in Fig. 2. All samples' XRD profiles display the distinctive diffraction peaks at rounds 18.3, 30.2, 35.6, 43.0, 53.5, 57.1, and 62.7°, which are attributed to the spinel ferrite type $CoFe_2O_4$ (JCPDS No. 22-1086) (111), (220), (311), (400), (422), (511), and (440) planes[120]. No impurity peaks were detected in any of the samples. The XRD of $CoFe_2O_4$/SBA-15 and $CoFe_2O_4$/SBA-15/CuPc@Gd reveal that the $CoFe_2O_4$ support remains structurally unchanged, this demonstrates the $CoFe_2O_4$'s phase preservation during the functionalization processes. $CoFe_2O_4$ magnetic nanoparticles retain their crystalline structure because the coated silica becomes amorphous. The diffraction peak at $2\theta = 71.0°$ in the XRD of the $CoFe_2O_4$/SBA-15/CuPc@Gd may result from species of metallic copper[121]. This peak was not observed in the XRD patterns for the $CoFe_2O_4$/SBA-15. The small angle XRD pattern of the mesoporous SBA-15 displays one strong peak indexed as (100) planes and two weak peaks corresponding to (110) and (200) planes of the 2D hexagonal mesoporous structure[122]. The low-angle XRD patterns of the $CoFe_2O_4$/SBA-15 and $CoFe_2O_4$/SBA-15/CuPc@Gd were also investigated as depicted in Fig. 3. The XRD pattern of the $CoFe_2O_4$/SBA-15 and $CoFe_2O_4$/SBA-15/CuPc@Gd gives only one peak at low angle corresponding to (100) plane, which indicated that the mesostructure was retained[123]. The two peaks corresponding to the (110) and (200) planes do not exist in the XRD patterns $CoFe_2O_4$/SBA-15 and $CoFe_2O_4$/SBA-15/CuPc@Gd. This result could be attributed to the lowering of local order[14].

FE-SEM, mapping, and HRTEM analysis

According to the HRTEM image, the $CoFe_2O_4$/SBA-15/CuPc@Gd showed a roughly spherical morphology with a gray SBA-15 and black CoFe2O4, suggesting that the $CoFe_2O_4$ is evenly distributed throughout the SBA-15 silica. HRTEM images of the $CoFe_2O_4$/SBA-15/CuPc show a pore wall region (Fig. 4). To illustrate the shape of the $CoFe_2O_4$/SBA-15 and $CoFe_2O_4$/SBA-15/CuPc@Gd, FE-SEM images were acquired (Fig. 5). The FE-SEM images of the $CoFe_2O_4$/SBA-15 and $CoFe_2O_4$/SBA-15/CuPc@Gd verify that SBA-15 particles and $CoFe_2O_4$ nanoparticles are present in the $CoFe_2O_4$/SBA-15, and $CoFe_2O_4$/SBA-15/CuPc@Gd composites. Figure 4 shows that the $CoFe_2O_4$ and CuPcS particles, which have an average size of roughly 15–30 nm, are fairly evenly distributed onto SBA-15.

To map the presence of elementals analysis, the EDS spectra and elemental mapping were used. The elemental mapping of the $CoFe_2O_4$/SBA-15/CuPc@Gd catalysts is given in Fig. 6. The desired elements are shown for $CoFe_2O_4$/SBA-15/CuPc@Gd. The EDS spectra for $CoFe_2O_4$/SBA-15/CuPc@Gd also shows the desired elements.
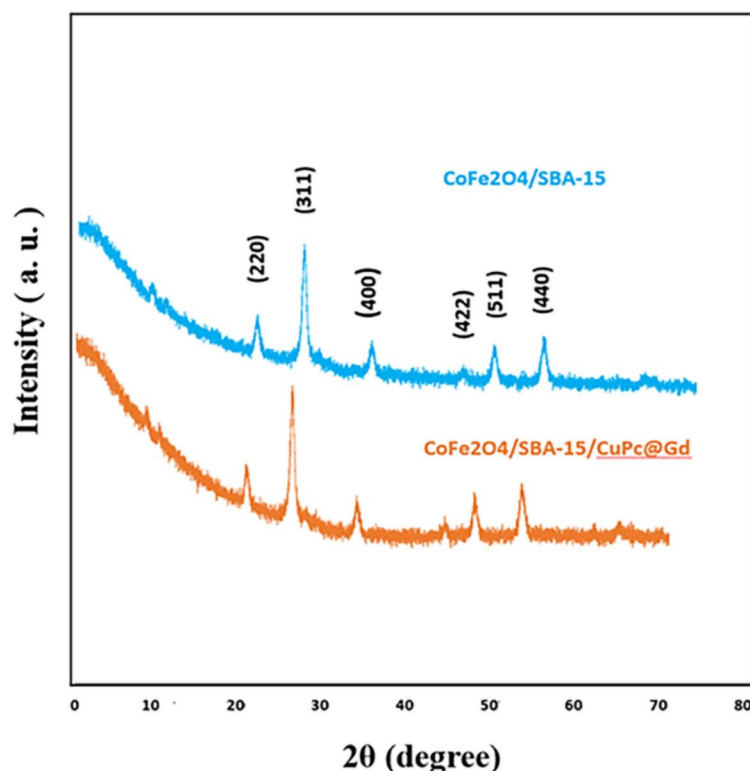
Fig. 2. Wide angle X-ray diffraction patterns of the $CoFe_2O_4$/SBA-15, and $CoFe_2O_4$/SBA-15/CuPc@Gd.
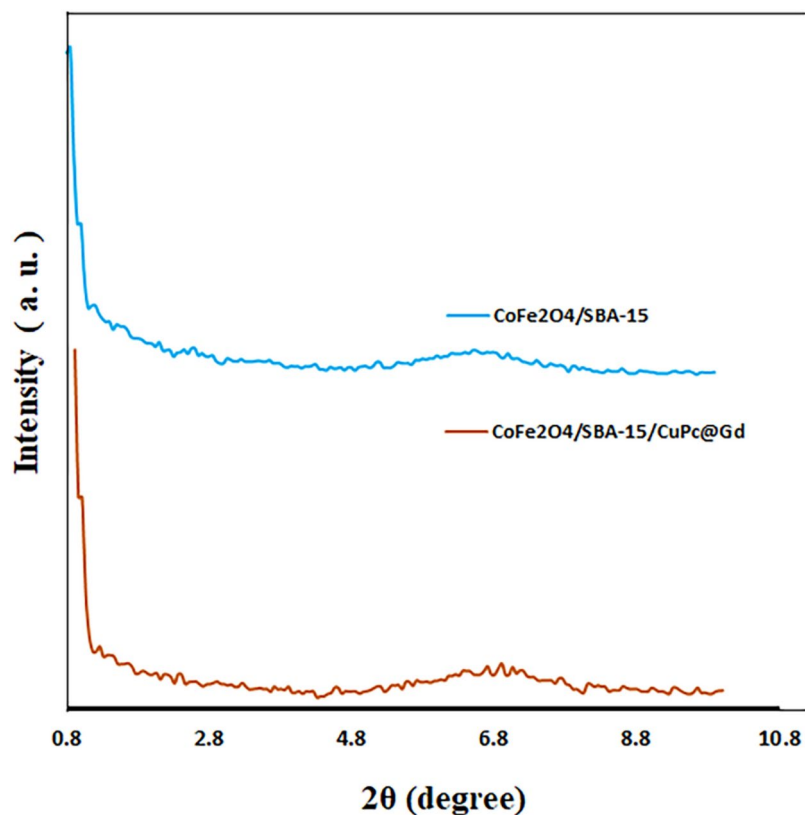
Fig. 3. Low angle X-ray diffraction patterns of the $CoFe_2O_4$/SBA-15, and $CoFe_2O_4$/SBA-15/CuPc@Gd.

Magnetic properties
Magnetization loops of $CoFe_2O_4$/SBA-15, and $CoFe_2O_4$/SBA-15/CuPc@Gd at the room-temperature are shown in Fig. 7. The samples' magnetization would almost reach saturation at 10,000 Oe of the applied magnetic field. $CoFe_2O_4$/SBA-15 had saturation magnetization (Ms) of 8.32 emu/g and remnant magnetization (Mr) of 2.25 emu/g, respectively, indicating a normal ferromagnetic hysteresis. As shown in the figure, the remnant magnetization (Mr), and saturation magnetization (Ms) values of $CoFe_2O_4$/SBA-15/CuPc@Gd magnetite particles are equal to 1.66 emu/g, and 6.08 emu/g respectively, which is lower than uncoated magnetite nanoparticles. This decrease in magnetism is due to the presence of a complex around $CoFe_2O_4$ nanoparticles.

N_2 adsorption–desorption isotherms
The BET and t-plot were used to measure the surface area, and the BJH method were used to examine the textural properties of $CoFe_2O_4$/SBA-15 and $CoFe_2O_4$/SBA-15/CuPc@Gd. The H1 hysteresis loop for a type IV adsorption–desorption isotherm which is seen in Fig. 8 demonstrates the presence of channels with a mesopore aspect in $CoFe_2O_4$/SBA-15, and $CoFe_2O_4$/SBA-15/CuPc@Gd[124]. The surface area (Brunauer–Emmett–Teller (S_{BET}) method), surface area (t-plot method (S t-Plot)), average pore sizes (d_{avg}) and total pore volumes (V_{total}) of $CoFe_2O_4$/SBA-15, and $CoFe_2O_4$/SBA-15/CuPc@Gd are shown in Table 2. Based on the given information, it can be observed that the BET and t-plot method show surface area of 158.89 m^2/g and 133.11 m^2/g respectively for $CoFe_2O_4$/SBA-15, also mean pore size is 7.00 nm, and pore volume is 0.276 cm^3/g. The $CoFe_2O_4$/SBA-15/CuPc@Gd shows a surface area by BET and t-plot of 122.2 m^2/g and 86.28 m^2/g respectively, with a mean pore size of 5.37 nm, and pore volume of 0.164 cm^3/g. The decrease in surface area signifies the binding of organic species on the mesopore surface and the decrease in the volume of the pores proves that the desired species is positioned inside the pores. Additionally, the distribution of BJH pore sizes was between 1 and 8 nm for the $CoFe_2O_4$/SBA-15 and 1–5 nm for the $CoFe_2O_4$/SBA-15/CuPc@Gd (Fig. 9).

FT-IR analysis
The infrared spectra of the synthesized samples were investigated and they can be seen in Fig. 10.

The signals at approximately 587 cm^{-1} in all curves correspond to the Fe–O bond's stretching modes. In the infrared spectrum of SBA-15, an absorption band is observed in the region of 1000–1300 cm^{-1} due to Si–O–Si asymmetric stretching vibrations.

The signals detected at about 463 cm^{-1} can be associated with the rocking motion of the bridging oxygens band in Si–O–Si, and the symmetric stretching vibration of Si–O–Si bonds can be coupled with the 803 cm^{-1}. The band at around 3200–3700 cm^{-1} is related to the surface hydroxyl groups stretching vibrations of the silanol group (Si–OH). The band at the 1623–1650 cm^{-1} region is due to the H–O–H bending vibration. In the infrared
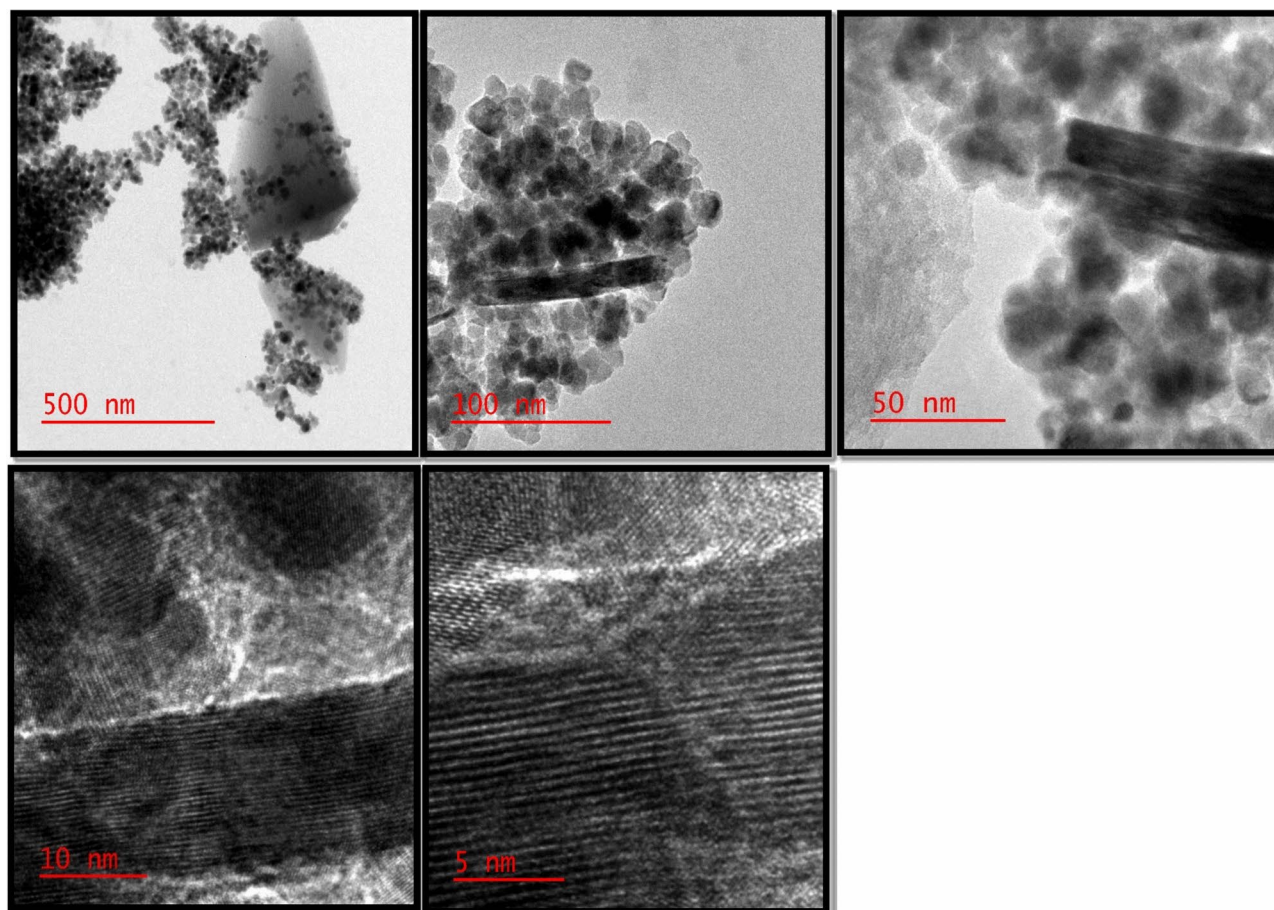
Fig. 4. HRTEM and EDX of $CoFe_2O_4$/SBA-15/CuPc@Gd.

spectrum of $CoFe_2O_4$/SBA-15 the extra band at 960–970 cm^{-1} appears, which is mostly attributed to the Si–OH vibration mode; however, when metals are added, the band becomes more intense and shifts to a lower wavenumber. It shows that SBA-15 silica has been added to the magnetite nanoparticles. In the reported article the FT-IR of CuPc, out-of-plane bending vibration of C–H bonds of the phenyl and porphyrin were related to bands at 735 and 845 cm^{-1}, respectively. Bands at 1113 and 1335 cm^{-1} were attributed to the C–H vibration of the porphyrin and phenyl, respectively. The 1437 and 1510 cm^{-1} bands can be corresponded to the C=C stretching vibration in porphyrin and phenyl ring, respectively. The 1628 cm^{-1} band may be attributed to the C=N stretching vibration in the porphyrin. Bands at 1635 cm^{-1} and 3430 cm^{-1} can be related to the bending and stretching vibrations of OH groups on the catalyst surface and water adsorbed on the surface[125]. After loading the CuPc, the new bands are observed in the FT-IR of the $CoFe_2O_4$/SBA-15. The new band around at 1422 cm^{-1} is related to the anchored complex copper phthalocyanine[126]. In the FT-IR spectrum of $CoFe_2O_4$/SBA-15/CuPc@Gd, the density of band at 1400 cm^{-1} attributed to C=C stretching vibration in porphyrin has increased.

Catalyst evaluation

The catalyst containing $CoFe_2O_4$/SBA-15 coated with Gd(III) copper phthalocyanine complex was used to prepare 5-substituted-1H-tetrazoles derivatives. The reaction of benzonitrile (1 mmol), catalyst, and NaN_3 (1.2 mmol) was chosen as a reaction sample. To optimize the reaction conditions, the efficiency of catalyst amounts, various solvents, and different temperatures have been studied.

Effect of solvent

Different solvents such as PEG (Poly (ethylene glycol), n-hexane, acetonitrile, EtOH, EtOH/water, and water in 1440 min were tested. The reaction yield in PEG was 68% (Table 3, entry 1). In acetonitrile solvent, the reaction yield was 40% (Table 3, entry 2). In hexane solvent, the reaction yield was 30% (Table 3, entry 3). In the EtOH solvent, the reaction yield was 60% (Table 3, entry 4). The reaction yield in EtOH/water (1:1) solvent is 62% (Table 3, entry 5). The reaction yield in the EtOH/water (2:1) solvent is 55% (Table 3, entry 6). The reaction in water solvent within 60 min, the yield was 65% (Table 3, entry 7). Accordingly, H_2O solvent was selected as the intended solvent for this method. The solvent dielectric constant has a major impact on the chemical intermediate's stabilization. Higher solvent dielectric constant reaction intermediates are stabilized by stronger ionic forces[127,128]. Water exhibited the greatest dielectric constant (80) of all the solvents, followed by acetonitrile
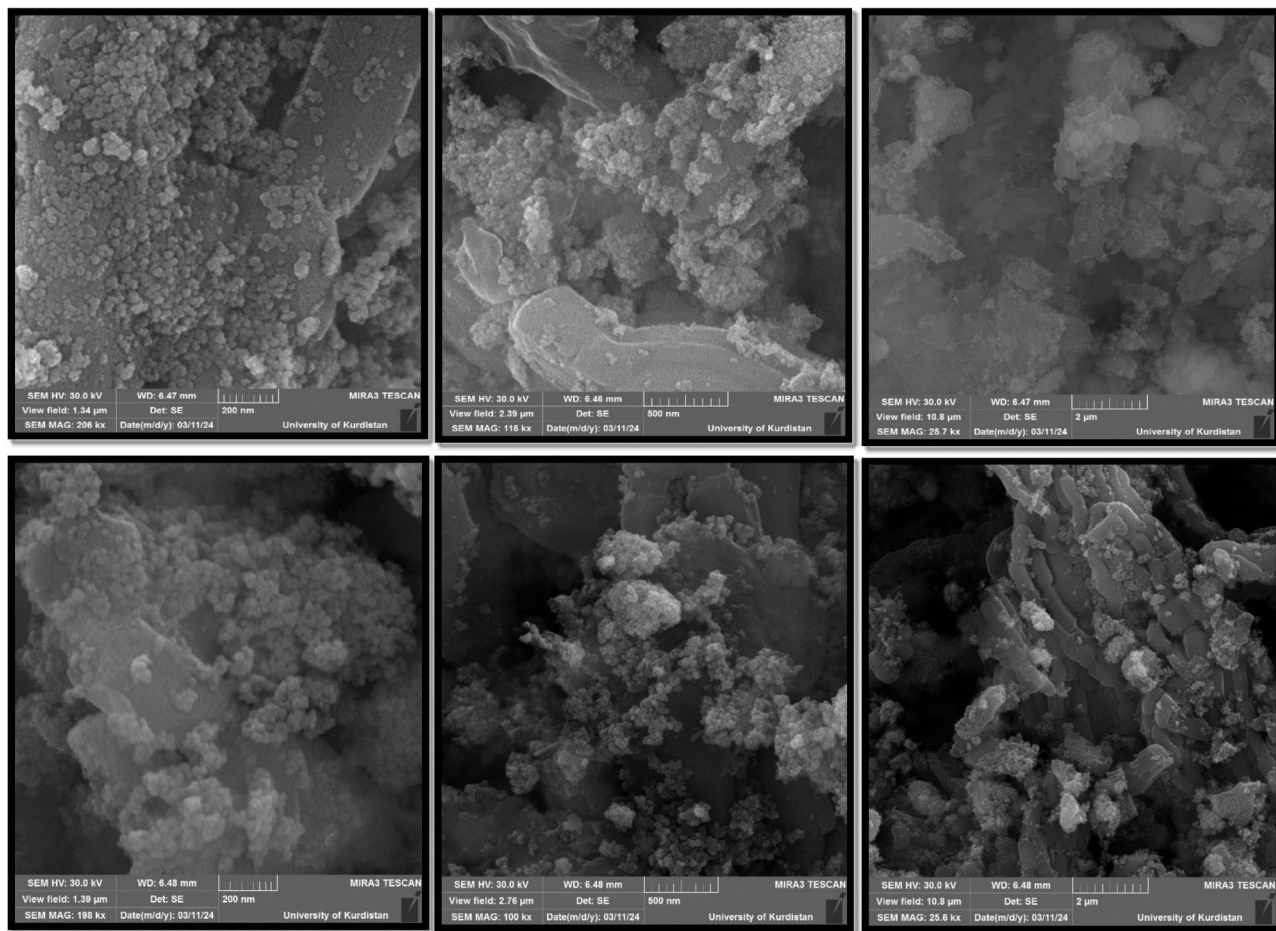
Fig. 5. SEM images of (up) $CoFe_2O_4$/SBA-15, and (down) $CoFe_2O_4$/SBA-15/CuPc@Gd.

(36.6), EtOH (24.3), and hexane (2.0), The degree of the reactants' solubility can be used to characterize the solvent impact. Derivatives of sodium azide dissolve more readily in water.

Effect of temperature
Different temperatures of Boling point, 60, and 40 ℃, were tested, based on Table 3 in H_2O solvent at boiling point, for 60 min the reaction yielded 65%. (Table 3, entry 7), and at a temperature of 60 °C in 80 min, the reaction yielded 57% (Table 3, entry 8), and at 40 °C in 120 min, the reaction yielded 55% (Table 3, entry 9). The temperature of the Boling point was chosen to continue the reaction process. The Arrhenius equation predicted that the reaction rate would rise with temperature[129]. The boiling point produced the best outcome for this reaction.

Effect of amounts of catalyst
The amount of catalyst was changed according to Table 3, and the value of 100 mg of catalyst was chosen (Table 3, entry 7). The abundance of active sites present in the sample framework is the cause of the maximal yield.

Using the optimized conditions, several tetrazole derivatives have been prepared with $CoFe_2O_4$/SBA-15/CuPc@Gd, which can be seen in Table 4. In this research, it has been tried to use different combinations of aromatic nitriles with electron withdrawing and electron donating groups. The ability to achieve successful conversion in a short time is a significant advantage of this method.

The formation of 1*H*-tetrazoles depends critically on the nitrile substrate's coordination with the Lewis acidic Gd (III). The Lewis acidic Gd (III) acts as an active site for the coordination of the nitrile molecule. The primary element affecting [2 + 3] cycloaddition is the coordination of Gd (III) to the nitrile. Tetrazole is the final result of further hydrolysis and azide nucleophilic assault. When the nitrile substrate coordinates with Gd^{3+}, it forms a stable complex that activates the nitrile toward nucleophilic attack. This coordination increases the electrophilicity of the carbon atom in the nitrile, making it more susceptible to nucleophilic attack by azide ions[130] (Scheme 1).

The oxidation of sulfides to sulfoxide for the catalytic activity of the catalysts was examined in the second section. A study was done on the best solvent to use, as well as the appropriate amount of catalyst and oxidant, to achieve the best conditions for carrying out the oxidation process of sulfides. For that, methyl phenyl sulfide oxidation was employed as a sample reaction at room temperature with various solvents in the presence of
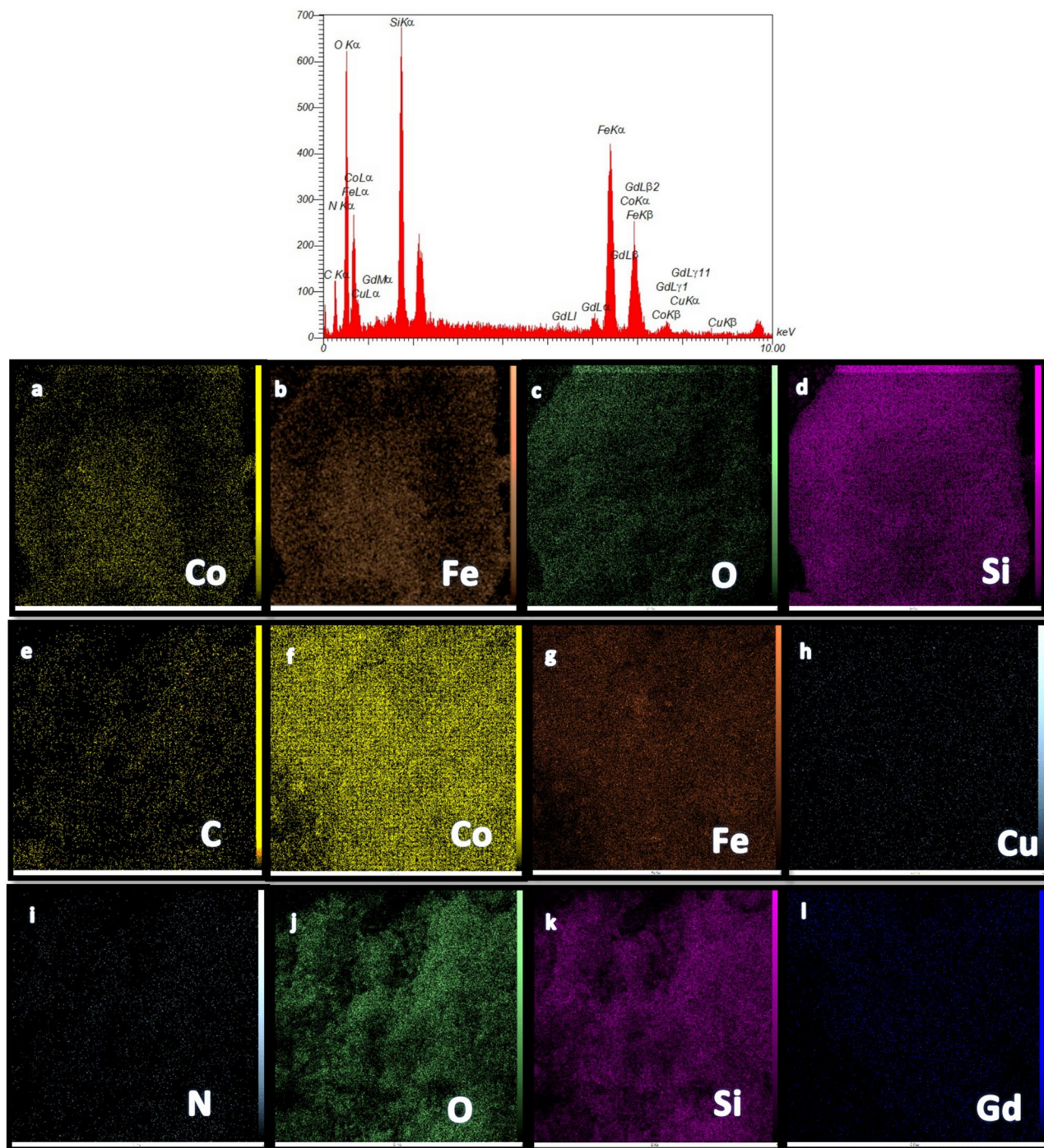
Fig. 6. EDX and Elemental mapping of (a-d) CoFe$_2$O$_4$/SBA-15, and (e-l) CoFe$_2$O$_4$/SBA-15/CuPc@Gd.

CoFe$_2$O$_4$/SBA-15/CuPc@Gd. Table 5 presents the survey's results. Initially, the reaction was screened using a variety of solvents, including acetonitrile, EtOH, and water. In this investigation, the maximum yield is seen in H$_2$O. The yields of the other solvents were lower.

The impact of catalyst weights (0, 4, 6, 8, and 10 mg) has also been investigated. The findings showed that the yield increased from 0% (0 mg) and 78% (4 mg) to 80% (6 mg) and finally to 91% (8 mg). The findings show that the catalyst's greatest yield was obtained at 8 mg, and that the product yields a little increased after 8 mg.

Additionally, we ran the process with varying concentrations of oxidant. The findings showed that the yield increased from 50% (0.1 mL), 80% (0.3 mL), and finally 91% (0.5 mL).

The most suitable amount required to complete this reaction was 8 mg of catalyst and 0.5 mL of H$_2$O$_2$, which produced the best results.
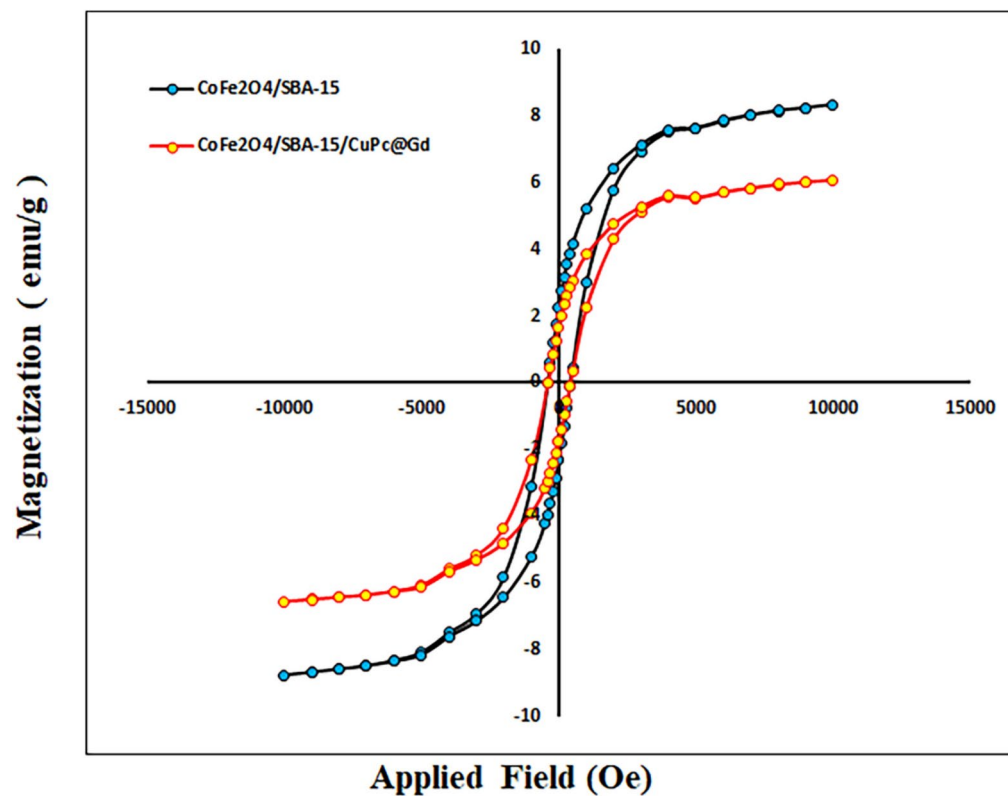
Fig. 7. Magnetization curves of CoFe$_2$O$_4$/SBA-15, and CoFe$_2$O$_4$/SBA-15/CuPc@Gd.
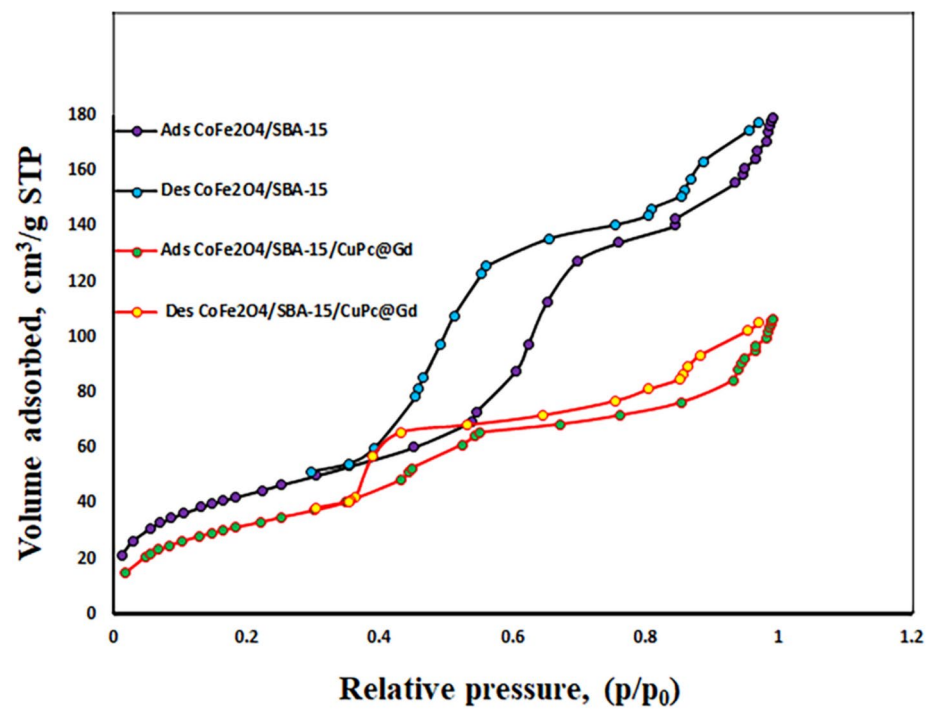
Fig. 8. N$_2$ adsorption–desorption isotherms of CoFe$_2$O$_4$/SBA-15, and CoFe$_2$O$_4$/SBA-15/CuPc@Gd.

Entry	Catalyst[b]	S_{BET} (m²/g)	$S_{t\text{-}Plot}$ (m²/g)	d_{avg} (nm)	V_{total} (cm³/g)
1	$CoFe_2O_4$/SBA-15	158.89	133.11	6.95	0.276
2	$CoFe_2O_4$/SBA-15/CuPc@Gd	122.2	86.28	5.37	0.164

Table 2. The study's synthesized samples' textural characteristics[a].
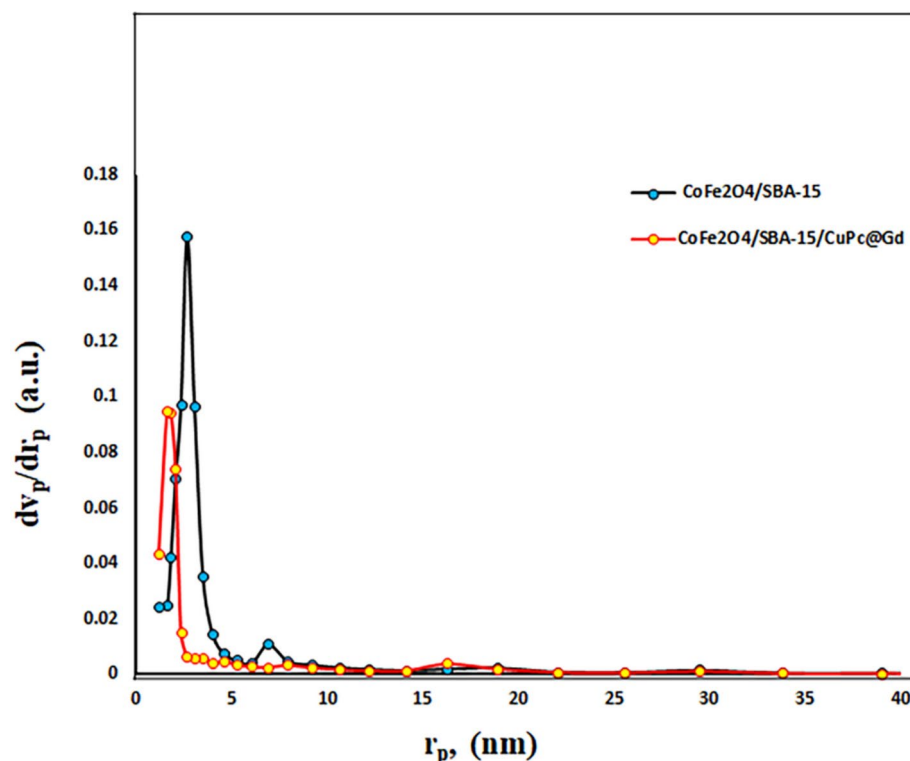
Fig. 9. BJH pore distribution of $CoFe_2O_4$/SBA-15, and $CoFe_2O_4$/SBA-15/CuPc@Gd.

After the ideal conditions had been achieved, as indicated in Table 6, a variety of sulfides with various functional groups were employed to produce sulfoxides, which resulted in the production of the intended products with a high yield and a short reaction time. This catalyst has been used to create both aliphatic and aromatic sulfoxides, as can be observed. These findings unequivocally demonstrate that this approach can be used to quickly and environmentally-friendly convert a wide range of derivatives, which is an enormous advantage in the field of green chemistry.

Based on the reported mechanism for the oxidation of sulfides into sulfoxides using hydrogen peroxide in the presence of a catalyst, one explanation for this process is the complex formation between the hydrogen peroxide and the M(III) (intermediate A). After the formation of [M^{III}-OOH], it may form oxo metal species as the active oxidant (intermediate B). This active species can oxidize organic sulfides by the formation of the oxidant-substrate complex (intermediate C) and the oxygen transfer to the organic substrate (Scheme 2 and 3)[133–136].

Homoselectivity and chemoselectivity

When there are two or more identical functional groups in a molecule, only one of them reacts selectively in the course of the reaction; this selectivity can be named homoselectivity[141,142]. $CoFe_2O_4$/SBA-15/CuPc@Gd catalyst shows a good homoselectivity in dicyano-functional benzonitriles, e.g., phthalonitrile (Table 4, entry 11) and terephthalonitrile (Table 4, entry 12) for the synthesis of corresponding tetrazoles (Scheme 4).

Chemoselectivity is the preferential reaction of one functional group in the presence of others[143,144]. Also, there is chemoselectivity in the oxidation of 2-(phenylthio) ethanol (Table 6, entry 6). In this substrate, the functional group of sulfide was converted to the sulfoxide, but alcohol oxidation did not occur during the conversion, and the primary hydroxyl group retained intact in the course of the reaction in the presence of H_2O_2 as oxidant (Scheme 5).

Catalyst reusability

The catalyst's capacity for recovery is one of the key responsibilities of green chemistry. After a reaction was completed, the catalyst was separated using a magnet and repeatedly rinsed with acetonitrile and ethanol for
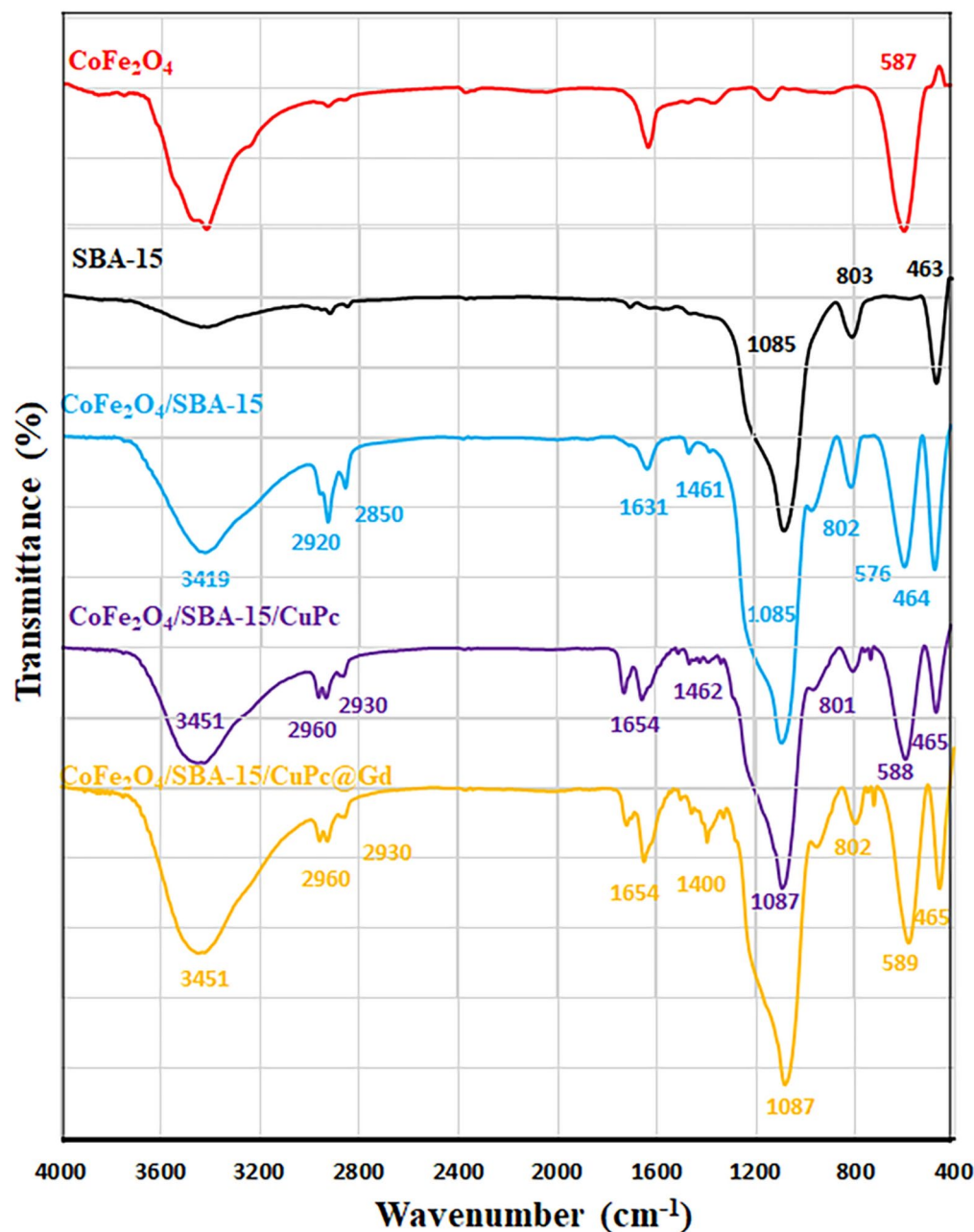
Fig. 10. FT-IR spectra of $CoFe_2O_4$, SBA-15, $CoFe_2O_4$/SBA-15, and $CoFe_2O_4$/SBA-15/CuPc@Gd.

catalyst recovery. Following an oven-drying process, it was reused in a fresh run with optimal parameters with benzonitrile (1 mmol), catalyst (100 mg), and NaN_3 (1.2 mmol), in an aqueous medium. The results for the heterogeneous catalyst that was used for the synthesis of tetrazole are shown in Fig. 11. As can be seen, without experiencing a significant reduction in its catalytic activity, the recovered catalyst was utilized five times in the process.

Leaching study

The leaching of the catalyst was investigated with ICP-AES (Inductively coupled plasma atomic emission spectroscopy). ICP-AES analysis of the fresh and recovered catalyst was investigated. Using the ICP-AES technique, the Gadolinium (Gd) quantity of the catalyst before and after the reaction for the preparation of 5-(4-chlorophenyl)-1*H*-tetrazole was determined. It was obtained that the quantity of Gadolinium (Gd) in the fresh $CoFe_2O_4$/SBA-15/CuPc@Gd catalyst is 0.7 mmol g^{-1}. Gadolinium (Gd) content has slightly decreased to 0.6 mmol g^{-1} after the 5th catalytic reaction cycle.

Entry	Solvent	Catalyst (mg)	Temperature (°C)	Time (min)	Yield (%)ᵃ
1	PEG	100	120	1440	68
2	Acetonitrile	100	82	1440	40
3	Hexane	100	68	1440	30
4	EtOH	100	75	1440	60
5	H_2O /EtOH (1:1)	100	75	1440	62
6	H_2O /EtOH (1:2)	100	75	1440	55
7	H_2O	100	Boiling point	60	65
8	H_2O	100	60	80	57
9	H_2O	100	40	120	55
10	H_2O	80	Boiling point	70	62
11	H_2O	60	Boiling point	90	59
12	H_2O	40	Boiling point	140	60
13	H_2O	–	Boiling point	1440	Trace

Table 3. 1*H*-tetrazole yield at different solvents, catalyst amounts, and temperatures in the presence of $CoFe_2O_4$/SBA-15/CuPc@Gd Reactions conditions: Nitrile (1 mmol), solvent (3 mL), catalyst, and NaN_3 (1.2 mmol). ᵃIsolated yield.

Conclusion

We have prepared $CoFe_2O_4$/SBA-15/CuPc@Gd the mesoporous catalysts for converting nitrile to tetrazole in a single pot and oxidation of sulfides. It is confirmed by the X-ray diffraction patterns of the spinel ferrite type for $CoFe_2O_4$/SBA-15/CuPc@Gd. The FE-SEM images of the $CoFe_2O_4$/SBA-15 and $CoFe_2O_4$/SBA-15/CuPc@Gd verify that SBA-15 particles and $CoFe_2O_4$ nanoparticles are present in the $CoFe_2O_4$/SBA-15, and $CoFe_2O_4$/SBA-15/CuPc@Gd composites. The $CoFe_2O_4$, CuPc, and Gd (III) particles, which have an average size of roughly 15–30 nm, are fairly evenly distributed onto SBA-15. The EDS spectra and elemental mapping show the desired elements for $CoFe_2O_4$/SBA-15/CuPc@Gd. The remnant magnetization (Mr) and saturation magnetization (Ms) values of $CoFe_2O_4$/SBA-15/CuPc@Gd magnetite particles are equal to 1.66 emu/g, and 6.08 emu/g respectively, which is lower than uncoated magnetite nanoparticles. The $CoFe_2O_4$/SBA-15/CuPc@Gd shows a surface area by BET and t-plot of 122.2 m^2/g and 86.28 m^2/g respectively, with a mean pore size of 5.37 nm, and pore volume of 0.164 cm^3/g. The catalyst was used for the synthesis of tetrazole in an aqueous medium. There is no reduction in the conversion of nitrile to tetrazole after the 5 cycles for $CoFe_2O_4$/SBA-15/CuPc@Gd. Also, the catalyst was used for the oxidation of sulfides to sulfoxide.
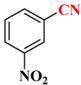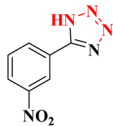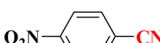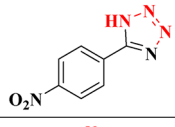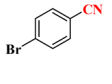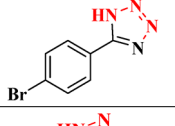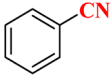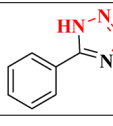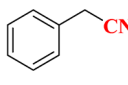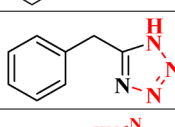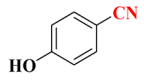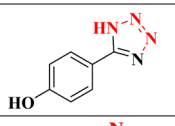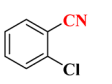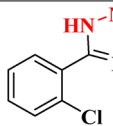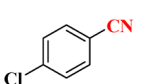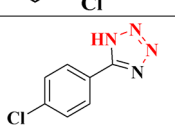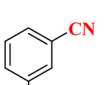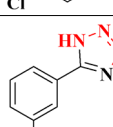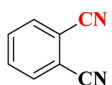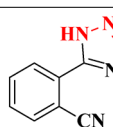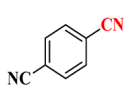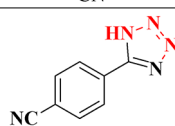
Entry	Substrate	Product	Time (min)	Yield (%)	TON[a]	TOF[b] (min⁻¹)	M. p (°C)
1	3-nitrobenzonitrile	tetrazole product	150	58	8.28	0.05	148–150 [93]
2	4-nitrobenzonitrile	tetrazole product	150	67	9.57	0.06	217–219 [93]
3	3-bromobenzonitrile	tetrazole product	90	55	7.85	0.09	182–184
4	4-bromobenzonitrile	tetrazole product	90	62	8.85	0.1	262–265 [131]
5	benzonitrile	tetrazole product	60	65	9.28	0.15	213–216 [93]
6	phenylacetonitrile	tetrazole product	120	58	8.28	0.07	122–125 [131]
7	4-hydroxybenzonitrile	tetrazole product	180	60	8.57	0.05	232–235 [132]
8	2-chlorobenzonitrile	tetrazole product	120	57	8.14	0.07	176–179 [93]
9	4-chlorobenzonitrile	tetrazole product	120	65	9.28	0.08	262–264 [93]
10	3-chlorobenzonitrile	tetrazole product	120	59	8.42	0.07	131–133 [131]
11	phthalonitrile	tetrazole product	50	78	11.14	0.56	210–212 [67]
12	terephthalonitrile	tetrazole product	45	80	11.43	0.25	250–253 [12]

Table 4. Synthesis of 5-substituted 1*H*-tetrazoles derivatives in the presence of $CoFe_2O_4$/SBA-15/CuPc@Gd. Reactions conditions: Nitrile (1 mmol), NaN_3 (1.2 mmol), H_2O (3 mL), and catalyst (100 mg). [a]TON, turnover number, moles of aryl halides converted per mole of Pd. [b]TOF, turnover frequencies, TON/time of reaction.
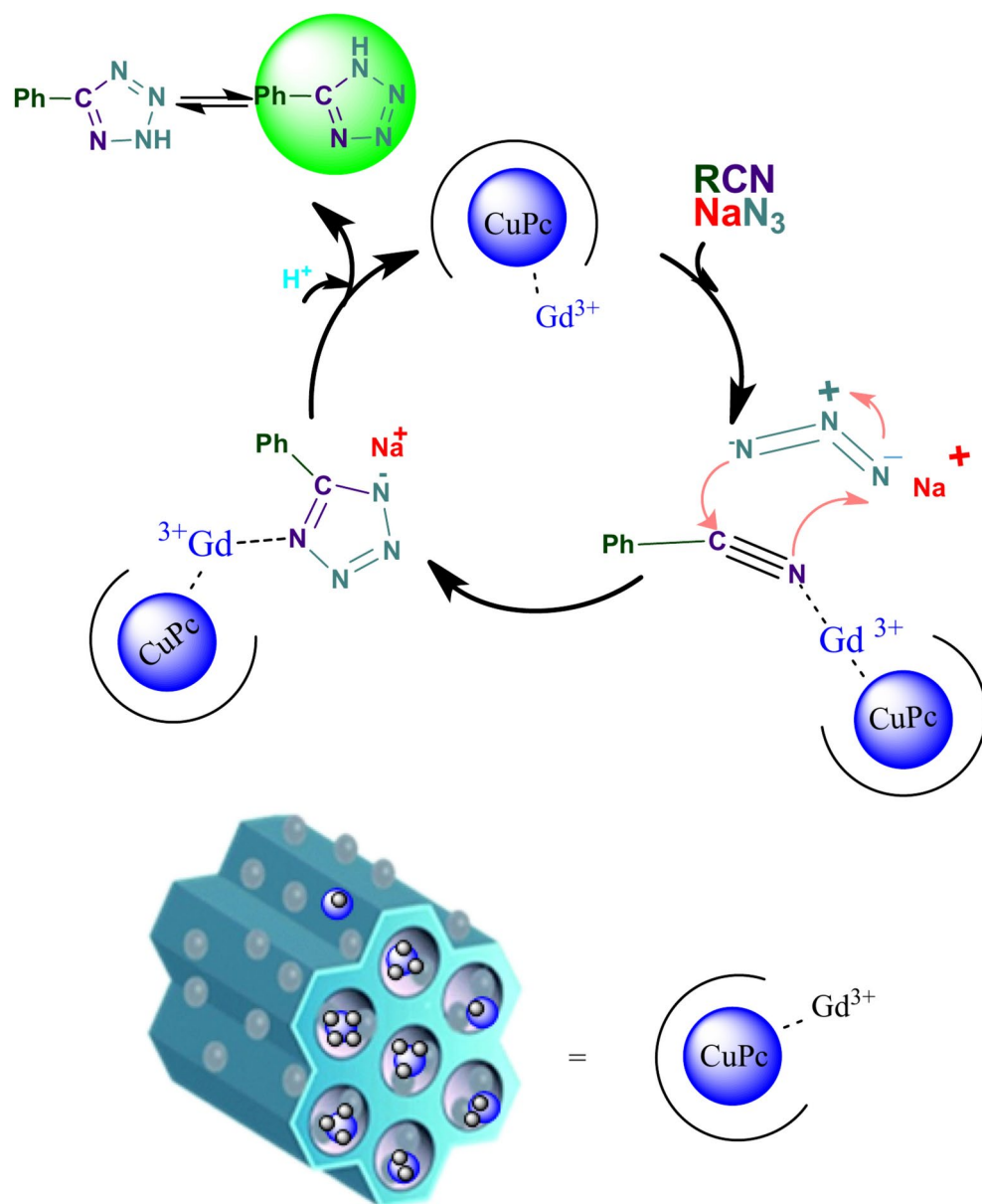
Scheme 1. Plausible Reaction Pathway for the Direct Conversion of over the CoFe$_2$O$_4$/SBA-15/CuPc@Gd Catalyst.

Entry	Solvent	Catalyst (mg)	H_2O_2 (mL)	Time (min)	Yield (%) [a]
1	Water	8	0.5	120	60
2	Ethyl acetate	8	0.5	120	35
3	ACN	8	0.5	120	45
4	EtOH	8	0.5	45	91
5	EtOH	10	0.5	45	93
6	EtOH	6	0.5	60	80
7	EtOH	4	0.5	120	78
8	EtOH	–	0.5	120	nil
9	EtOH	8	0.3	55	80
10	EtOH	8	0.1	70	50

Table 5. Optimization of reaction parameters for the synthesis sulfoxide. Reaction conditions: Sulfide (1 mmol), H_2O_2, catalyst, and solvent (3 mL). [a]Isolated yield.
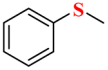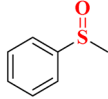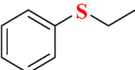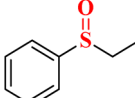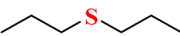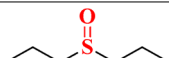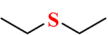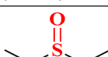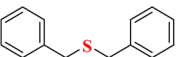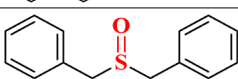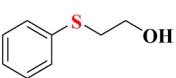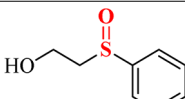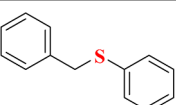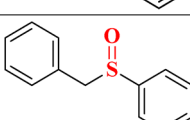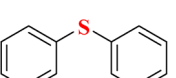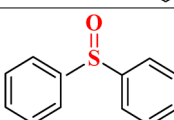
Entry	Substrate	Product	Time (min)	Yield (%)	TON	TOF	M. p (°C)
1			20	85	12.12	0.61	Oil [137]
2			45	89	12.70	0.28	Oil [138]
3			25	80	11.40	0.46	Oil [131]
4			20	88	12.54	0.63	Oil [131]
5			30	65	9.27	0.31	129–131 [139]
6			60	80	11.41	0.19	Oil [137]
7			25	75	10.70	0.43	116–118 [140]
8			30	65	9.27	0.31	63–65 [139]

Table 6. Synthesis of sulfoxides derivatives in the presence of CoFe$_2$O$_4$/SBA-15/CuPc@Gd. Reactions conditions: Sulfide (1 mmol), catalyst (5 mg), and H_2O_2 (0.5 mL) as oxidant at room temperature.
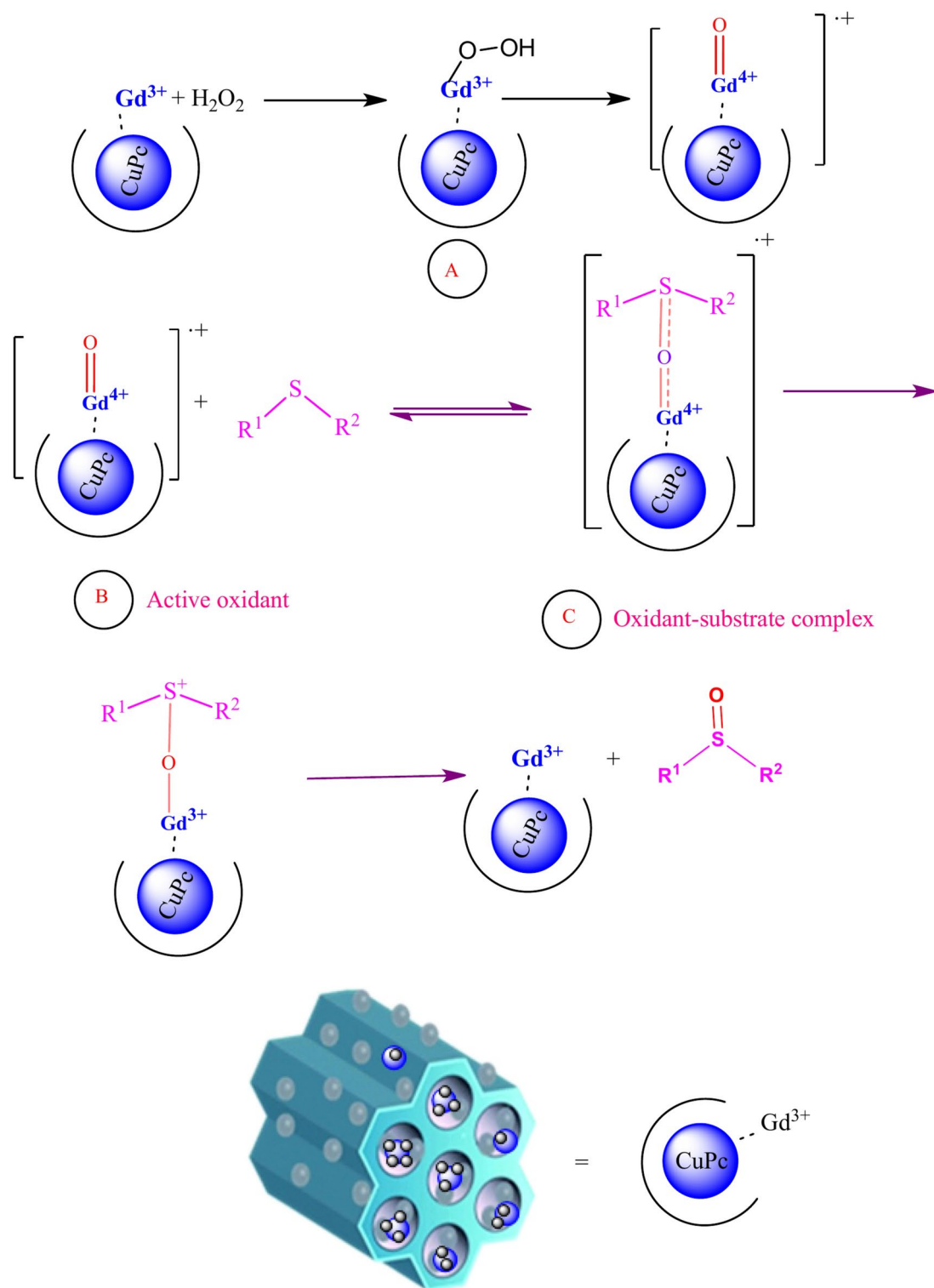
Scheme 2. Oxygen atom transfer mechanism for the selective oxidation of sulfides to sulfoxide.
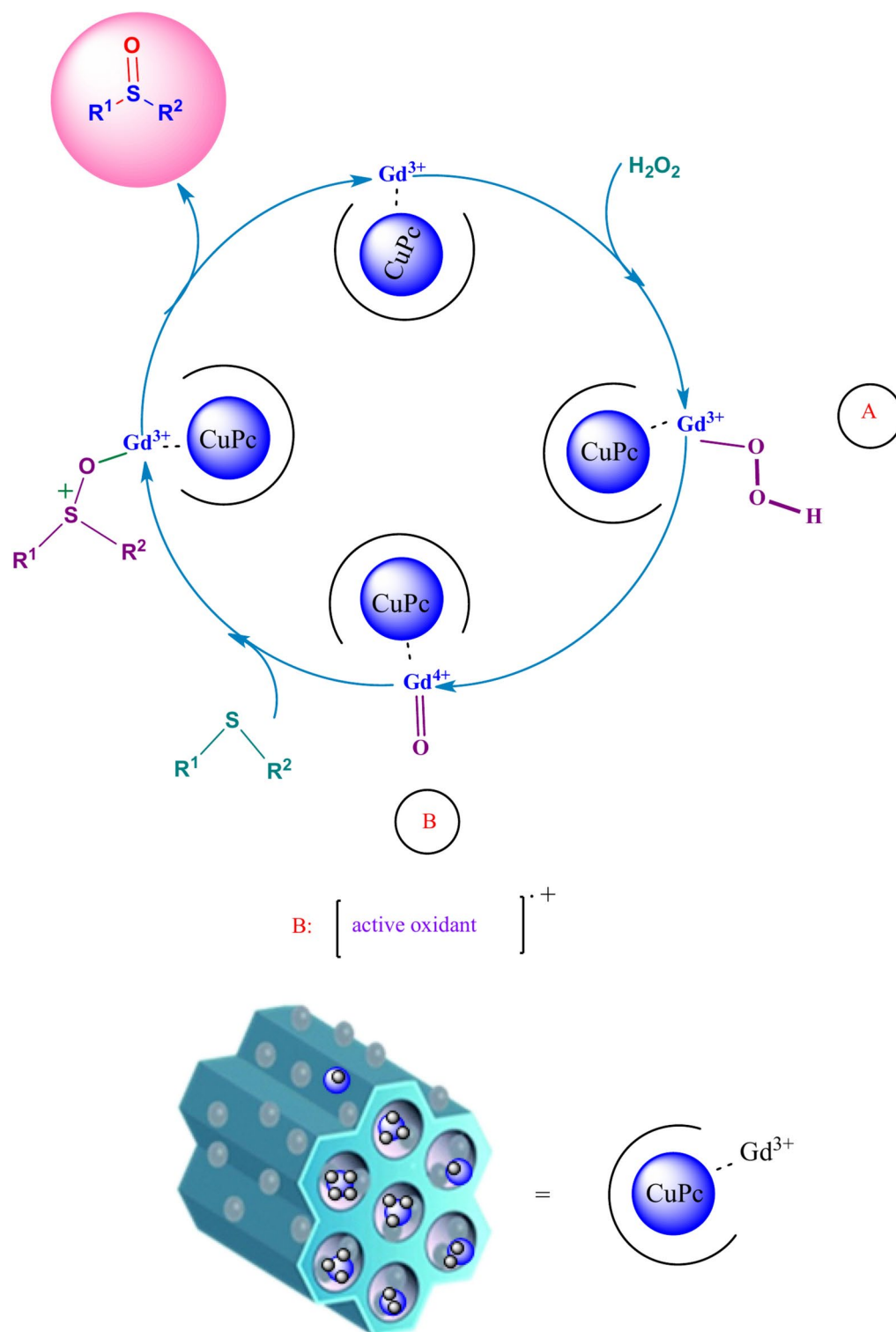
Scheme 3. A plausible mechanism for sulfoxide formation reactions using H_2O_2 over $CoFe_2O_4$/SBA-15/ CuPc@Gd catalyst.
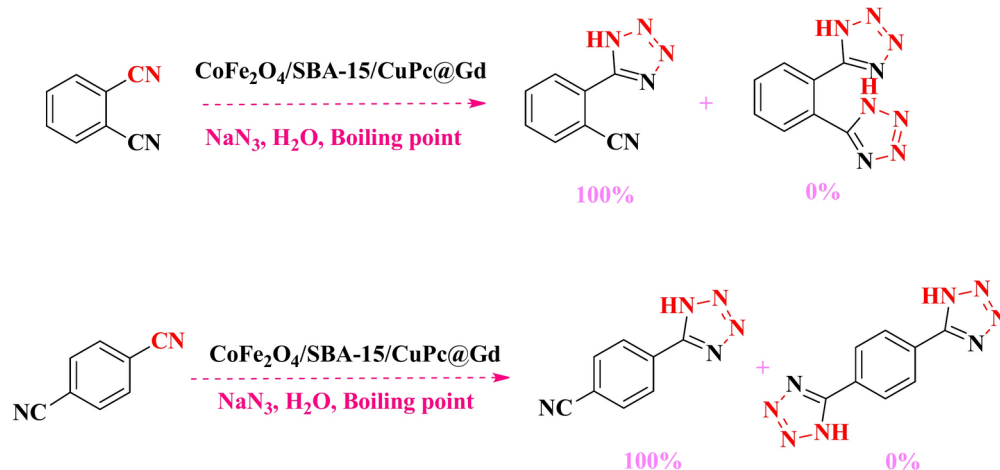
Scheme 4. Homoselectivity of CoFe$_2$O$_4$/SBA-15/CuPc@Gd in the synthesis of tetrazoles.
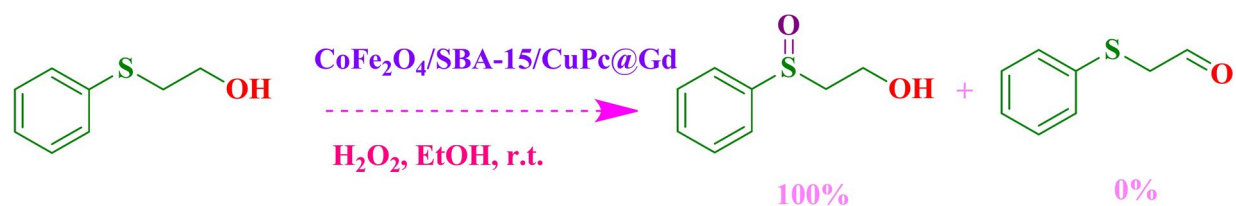
Scheme 5. Chemoselective sulfoxidation of 2-(phenylthio) ethanol.
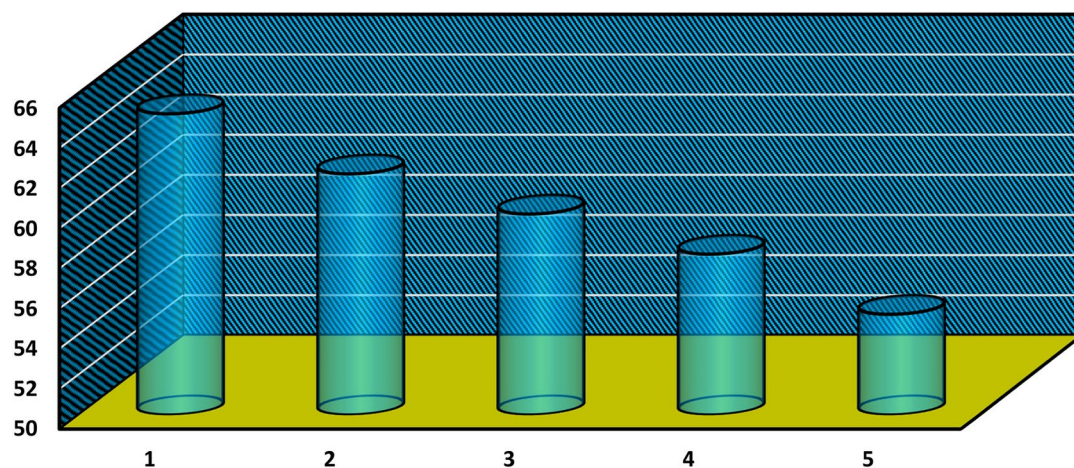
Fig. 11. Reusability of the CoFe$_2$O$_4$/SBA-15/CuPc@Gd.

Data availability

The datasets used and/or analyzed during the current study are available from the corresponding author upon reasonable request.

References

1. Samadi Khoshkhoo, M. et al. Surface functionalization with copper tetraaminophthalocyanine enables efficient charge transport in indium tin oxide nanocrystal thin films. *ACS Appl. Mater. Interfaces* **9**(16), 14197–14206 (2017).
2. Figueira, F. et al. Synthesis and anion binding properties of porphyrins and related compounds. *J. Porphyr. Phthalocyanines* **20**, 950–965 (2016).

19

3. Castro, K. A. D. F. et al. Copper-phthalocyanine coordination polymer as a reusable catechol oxidase biomimetic catalyst. *Dalton Trans.* **48**, 8144–8152 (2019).

4. Arellano, L. M. et al. Edge-on and face-on functionalized Pc on enriched semiconducting SWCNT hybrids. *Nanoscale* **10**, 5205–5213 (2018).

5. Claessens, C. G., Hahn, U. W. E. & Torres, T. Phthalocyanines: From outstanding electronic properties to emerging applications. *Chem. Rec.* **8**, 75–97 (2008).

6. Sorokin, A. B. Phthalocyanine metal complexes in catalysis. *Chem. Rev.* **113**, 8152–8191 (2013).

7. Fernandez, L., Esteves, V. I., Cunha, A., Schneider, R. J. & Tome, J. P. C. Photodegradation of organic pollutants in water by immobilized porphyrins and phthalocyanines. *J. Porphyr. Phthalocyanines* **20**, 150–166 (2016).

8. Mahmiani, Y., Sevim, A. M & Gül, A. Photocatalytic degradation of 4-chlorophenol under visible light by using TiO_2 catalysts impregnated with Co(II) and Zn(II) phthalocyanine derivatives. *J. Photochem. Photobiol. A* **321**, 24–32 (2016).

9. Alves, E. et al. A new insight on nanomagnet–porphyrin hybrids for photodynamic inactivation of microorganisms. *Dyes Pigm.* **110**, 80–88 (2014).

10. Castro, K. ADd. F. et al. Synthesis of new metalloporphyrin derivatives from [5,10,15,20-tetrakis (pentafluorophenyl)porphyrin] and 4-mercaptobenzoic acid for homogeneous and heterogeneous catalysis. *Appl. Catal. A.* **503**, 9–19 (2015).

11. Castro, K. A. D. F. et al. Glycol metalloporphyrin derivatives in solution or immobilized on LDH and silica: Synthesis, characterization and catalytic features in oxidation reactions. *Catal. Sci. Technol.* **4**, 129–141 (2014).

12. Maseer, M. M., Kikhavani, T. & Tahmasbi, B. A multidentate copper complex on magnetic biochar nanoparticles as a practical and recoverable nanocatalyst for the selective synthesis of tetrazole derivatives. *Nanoscale Adv.* **6**(5), 3948–3960 (2024).

13. Norouzi, M. & Moradi, P. A new copper complex on functionalized magnetic biochar nano-sized materials as sustainable heterogeneous catalysts for C-O bond formation in the natural deep eutectic solvent. *Biomass Convers. Biorefinery* **15**(2), 2465–2477 (2025).

14. Ahmadi, A., Sedaghat, T., Motamedi, H. & Azadi, R. Anchoring of Cu(II)-Schiff base complex on magnetic mesoporous silica nanoparticles: Catalytic efficacy in one-pot synthesis of 5-substituted-1H-tetrazoles, antibacterial activity evaluation and immobilization of α-amylase. *Appl. Organomet. Chem.* **34**, e5572 (2020).

15. Moradi, P. Investigation of Fe_3O_4 @boehmite NPs as efficient and magnetically recoverable nanocatalyst in the homoselective synthesis of tetrazoles. *RSC Adv.* **12**, 33459–33468 (2022).

16. Ghasemirad, M., Norouzi, M. & Moradi, P. A novel Cu complex coated on hercynite magnetic nanoparticles as an efficient and recoverable nanocatalyst for the selective synthesis of tetrazoles. *J. Nanoparticle Res.* **26**, 14 (2024).

17. Rostami, A. et al. Silica sulfuric acid-coated Fe_3O_4 nanoparticles as high reusable nanocatalyst for the oxidation of sulfides into sulfoxides, protection and deprotection of hydroxyl groups using HMDS and Ac_2O. *J. Saudi Chem. Soc.* **21**, 399–407 (2017).

18. Wang, L., Xu, S., He, S. & Xiao, F.-S. Rational construction of metal nanoparticles fixed in zeolite crystals as highly efficient heterogeneous catalysts. *Nano Today* **20**, 74–83 (2018).

19. Altava, B., Burguete, M. I., García-Verdugo, E. & Luis, S. V. Chiral catalysts immobilized on achiral polymers: effect of the polymer support on the performance of the catalyst. *Chem. Soc. Rev.* **47**, 2722–2771 (2018).

20. Ye, Z. et al. Exceptional adsorption and catalysis effects of hollow polyhedra/carbon nanotube confined CoP nanoparticles superstructures for enhanced lithium–sulfur batteries. *Nano Energy* **64**, 103965 (2019).

21. Sarvestani, M. & Azadi, R. Buchwald–Hartwig amination reaction of aryl halides using heterogeneous catalyst based on Pd nanoparticles decorated on chitosan functionalized graphene oxide. *Appl. Organomet. Chem.* **32**, e3906 (2018).

22. Tahmasbi, B., Darabi, M., Moradi, P., Tyula, Y. A. & Nikoorazm, M. Gadolinium Schiff-base complex on nanocomposite of graphene oxide magnetic nanoparticles as a robust, reusable and chemoselective nanocatalyst in the C–C coupling reactions. *Polyhedron* **258**, 117038 (2024).

23. Nikoorazm, M. et al. Synthesis and characterization of a new Schiff-base complex of copper on magnetic MCM-41 nanoparticles as efficient and reusable nanocatalyst in the synthesis of tetrazoles. *Polyhedron* **244**, 116587 (2023).

24. Tahmasbi, B., Moradi, P. & Darabi, M. A new neodymium complex on renewable magnetic biochar nanoparticles as an environmentally friendly, recyclable and efficient nanocatalyst in the homoselective synthesis of tetrazoles. *Nanoscale Adv.* **6**, 1932–1944 (2024).

25. Moradi, P., Zarei, B., Abbasi Tyula, Y. & Nikoorazm, M. Novel neodymium complex on MCM-41 magnetic nanocomposite as a practical, selective, and returnable nanocatalyst in the synthesis of tetrazoles with antifungal properties in agricultural. *Appl. Organomet. Chem.* **37**, e7020 (2023).

26. Huh, S. et al. Organic functionalization and morphology control of mesoporous silicas via a co-condensation synthesis method. *Chem. Mater.* **15**(22), 4247–4256 (2003).

27. Xia, Y., Yang, Z. & Mokaya, R. Molecularly ordered ethylene-bridged periodic mesoporous organosilica spheres with tunable micrometer sizes. *Chem. Mater.* **18**, 1141–1148 (2006).

28. Molaei, S. & Ghadermazi, M. Introduction of Ni into mesoporous MCM-41: A new recyclable catalyst for the synthesis of 5-substituted 1 H-tetrazoles and the selective oxidation of sulfides. *J. Porous Mater.* **29**, 1929–1945 (2022).

29. Ghadermazi, M. & Molaei, S. Synthesis of Sm(III) complex immobilized in MCM-41: A new heterogeneous catalyst for the facile synthesis of 5-substituted 1H-tetrazoles via [3+2] cycloaddition of nitriles and sodium azide. *Inorg. Chem. Commun.* **147**, 110225 (2023).

30. Ghadermazi, M., Molaei, S. & Mousavipour, S. M. Nano architectonics of Fe–Cu bimetallic particles confined in a mesoporous silica network for the synthesis of 5-substituted 1*H*-tetrazoles. *J. Inorg. Organomet. Polym. Mater.* **33**, 3128–3145 (2023).

31. Neouze, M.-A. About the interactions between nanoparticles and imidazolium moieties: Emergence of original hybrid materials. *J. Mater. Chem.* **20**, 9593–9607 (2010).

32. Kalbasi, R. J., Kolahdoozan, M., Massh, A. & Shahabian, K. ChemInform abstract: Synthesis, characterization and application of poly(4-methyl vinylpyridinium hydroxide)/SBA-15 composite as a highly active heterogeneous basic catalyst for the Knoevenagel reaction.. *ChemInform* https://doi.org/10.1002/chin.201108083 (2011).

33. Ghadermazi, N., Molaei, S. & Ghadermazi, M. Formation of Iron/MCM-41 nanocomposites with trifunctional ligand via dodecyl trimethylammonium bromide (DTAB) surfactant: Two heterogeneous catalysts for the green synthesis of 5-substituted 1H-tetrazoles. *Catal. Surv. Asia* **27**, 246–259 (2023).

34. Molaei, S. & Ghadermazi, M. Copper-decorated core–shell structured ordered mesoporous containing cobalt ferrite nanoparticles as high-performance heterogeneous catalyst toward synthesis of tetrazole. *Sci. Rep.* **13**, 15146 (2023).

35. Li, X.-K., Ji, W.-J., Zhao, J., Zhang, Z. & Au, C.-T. A comparison study on the partial oxidation of n-butane and propane over VPO catalysts supported on SBA-15, MCM-41, and fumed SiO2. *Appl. Catal. A: Gen.* **306**, 8–16 (2006).

36. Martín-Aranda, R. M. & Čejka, J. Recent advances in catalysis over mesoporous molecular sieves. *Top. Catal.* **53**, 141–153 (2010).

37. Krishnan, P. S., Tamizhdurai, P., Theres, G. S. & Shanthi, K. Molybdenum hybrid—Nanocrystals supported on modified Laponite composite as superior catalyst for vapour phase hydrodeoxygenation of clove oil. *Renew. Energy.* **148**, 451–466 (2020).

38. Ghadermazi, M. & Molaei, S. Synthesis of SBA-15@ 3, 4, 5-tri hydroxyphenyl acetic@ Tb for the facile synthesis of 5-substituted 1 H-tetrazoles. *Catal. Surv. Asia* **27**(2), 139–146 (2023).

39. Verma, P., Kuwahara, Y., Mori, K., Raja, R. & Yamashita, H. Functionalized mesoporous SBA-15 silica: Recent trends and catalytic applications. *Nanoscale* **12**, 11333–11363 (2020).

40. Abid, Z. et al. Preparation of highly hydrophilic PVA/SBA-15 composite materials and their adsorption behavior toward cationic dye: Effect of PVA content. *J. Mater. Sci.* **54**, 7679–7691 (2019).

41. Zhai, Q.-Z. & Li, X.-D. Modeling adsorption mechanism of paraquat onto Ayous (Triplochiton scleroxylon) wood sawdust. *Appl. Water Sci.* **9**, 1–11 (2019).
42. Yang, H.-C. et al. Recovery of uranium phosphate by a stepwise thermal treatment of uranium-bearing spent TBP. *J. Mater. Cycle. Waste Manag.* **18**, 437–444 (2016).
43. Zhang, Y. et al. Enhanced desulfurization performance of hybrid membranes using embedded hierarchical porous SBA-15. *Front. Chem. Sci. Eng.* **14**, 661–672 (2020).
44. Rodriguez-Estupinan, P., Correa-Navarro, Y. M., Vargas, D. P., Giraldo, L. & Moreno-Piraján, J. C. Enthalpies of immersion in caffeine and glyphosate aqueous solutions of SBA-15 and amino-functionalized SBA-15. *ACS Omega* **6**, 21339–21349 (2021).
45. Piché, D. et al. Targeted T 1 Magnetic Resonance Imaging Contrast Enhancement with Extraordinarily Small CoFe2O4 Nanoparticles. *ACS Appl. Mater. Interfaces.* **11**(7), 6724–6740 (2019).
46. Georgiadou, V. et al. Targeted T1 magnetic resonance imaging contrast enhancement with extraordinarily small CoFe$_2$O$_4$ nanoparticles. *Mater. Interfaces* **8**, 9345–9360 (2016).
47. Meidanchi, A. & Akhavan, O. Superparamagnetic zinc ferrite spinel–graphene nanostructures for fast wastewater purification. *Carbon* **69**, 230–238 (2014).
48. Fu, G. & Lee, J.-M. Ternary metal sulfides for electrocatalytic energy conversion. *J. Mater. Chem. A.* **7**, 9386–9405 (2019).
49. Masa, J. et al. *Adv. Energy Mater.* **6**, 1502313 (2016).
50. Liu, L. et al. From core–shell to yolk–shell: Improved catalytic performance toward CoFe2O4@ Hollow@ mesoporous TiO2 toward selective oxidation of styrene. *Ind. Eng. Chem. Res.* **59**(45), 19938–19951 (2020).
51. Moeini, N., Molaei, S. & Ghadermazi, M. Selective oxidation of sulfides and synthesis of 5-substituted 1 H-tetrazoles on Ce (III) immobilized CoFe2O4 as a magnetically separable, highly active, and reusable nanocatalyst. *Res. Chem. Intermed.* **48**(7), 3109–3128 (2022).
52. Sheykhan, M., Mohammadnejad, H., Akbari, J. & Heydari, A. Superparamagnetic magnesium ferrite nanoparticles: a magnetically reusable and clean heterogeneous catalyst. *Tetrahedron Lett.* **53**(24), 2959–2964 (2012).
53. Zhang, X. et al. Excellent low-temperature catalytic performance of nanosheet Co-Mn oxides for total benzene oxidation. *Appl. Catal. A General* **566**, 104–112 (2018).
54. Sun, Y. et al. Synthesis and magnetic properties of crystalline mesoporous CoFe2O4 with large specific surface area. *J. Mater. Chem.* **20**(5), 945–952 (2010).
55. Mohapatra, S., Rout, S. R., Maiti, S., Maiti, T. K. & Panda, A. B. Monodisperse mesoporous cobalt ferrite nanoparticles: synthesis and application in targeted delivery of antitumor drugs. *J. Mater. Chem.* **21**(25), 9185–9193 (2011).
56. Nidhin, M. et al. Flower shaped assembly of cobalt ferrite nanoparticles: application as T2 contrast agent in MRI. *RSC Adv.* **3**(19), 6906–6912 (2013).
57. Zavaliche, F. et al. Electrically assisted magnetic recording in multiferroic nanostructures. *Nano Lett.* **7**(6), 1586–1590 (2007).
58. Benson, F. R. The chemistry of the tetrazoles. *Chem. Rev.* **41**(1), 1–61 (1947).
59. Darabi, M., Nikoorazm, M., Tahmasbi, B. & Ghorbani-Choghamarani, A. *RSC adv.* **13**, 12572–12588 (2023).
60. Moradi, P., Kikhavani, T. & Abbasi Tyula, Y. A new samarium complex of 1,3-bis(pyridin-3-ylmethyl)thiourea on boehmite nanoparticles as a practical and recyclable nanocatalyst for the selective synthesis of tetrazoles. *Sci. Rep.* **13**, 5902 (2023).
61. Darabi, M., Nikoorazm, M., Tahmasbi, B. & Ghorbani-Choghamarani, A. Homoselective synthesis of tetrazole derivatives using copper complex anchored on mesoporous KIT-6 as a reusable, highly efficient, and environmentally green nanocatalyst. *Appl. Organo met. Chem.* **38**(4), e7392 (2024).
62. Norouzi, M., Moradi, P. & Khanmoradi, M. Aluminium-based ionic liquid grafted on biochar as a heterogeneous catalyst for the selective synthesis of tetrazole and 2, 3-dihydroquinazolin 4 (1 H)-one derivatives. *RSC Adv.* **13**(50), 35569–35582 (2023).
63. Molaei, S., Tamoradi, T., Ghadermazi, M. & Ghorbani-Choghamarani, A. Ordered mesoporous SBA-15 functionalized with yttrium(III) and cerium(III) complexes: Towards active heterogeneous catalysts for oxidation of sulfides and preparation of 5-substituted 1H-tetrazoles. *Appl. Organomet. Chem.* **33**, e4649 (2019).
64. Swami, S., Sahu, S. N. & Shrivastava, R. Nanomaterial catalyzed green synthesis of tetrazoles and its derivatives: a review on recent advancements. *RSC Adv.* **11**, 39058–39086 (2021).
65. Akbari, M., Nikoorazm, M., Tahmasbi, B. & Ghorbani-Choghamarani, A. The new Schiff-base complex of copper(II) grafted on mesoporous KIT-6 as an effective nanostructure catalyst for the homoselective synthesis of various tetrazoles. *Appl. Organo met. Chem.* **38**, e7317 (2024).
66. Mohseni, E., Ghorbani-Choghamarani, A., Tahmasbi, B. & Norouzi, M. A new Schiff base 2-benzoylpyridine-based copper complex on boehmite nanoparticles as a recoverable nanocatalyst for the homoselective synthesis of 5-substituted tetrazoles. *RSC Adv.* **14**, 16269–16277 (2024).
67. Tahmasbi, B., Nikoorazm, M., Moradi, P. & Tyula, Y. A. A Schiff base complex of lanthanum on modified MCM-41 as a reusable nanocatalyst in the homoselective synthesis of 5-substituted 1H-tetrazoles. *RSC Adv.* **12**, 34303–34317 (2022).
68. Alekasir, M., Heydarian, S. & Tahmasbi, B. The synthesis of biochar from biomass waste recycling and its surface modification for immobilization of a new Cu complex as a reusable nanocatalyst in the homoselective synthesis of tetrazoles. *Res. Chem. Intermed.* **50**, 2031–2049 (2024).
69. Jabbari, A., Moradi, P. & Tahmasbi, B. Synthesis of tetrazoles catalyzed by a new and recoverable nanocatalyst of cobalt on modified boehmite NPs with 1,3-bis(pyridin-3-ylmethyl)thiourea. *RSC Adv.* **13**, 8890–8900 (2023).
70. Tyula, Y. A., Moradi, P. & Nikoorazm, M. A new neodymium complex on boehmite nanoparticles with 1, 3-bis (pyridine-3-ylmethyl) thiourea as a practical and reusable nanocatalyst for the chemoselective synthesis of tetrazoles. *ChemistrySelect* **8**, e202301674 (2023).
71. Kikhavani, T., Moradi, P., Mashari-Karir, M. & Naji, J. A new copper Schiff-base complex of 3, 4-diaminobenzophenone stabilized on magnetic MCM-41 as a homoselective and reusable catalyst in the synthesis of tetrazoles and pyranopyrazoles. *Appl. Organomet. Chem.* **36**, e6895 (2022).
72. Hao, L., Stoian, S. A., Weddle, L. R. & Zhang, Q. Zr-Based MOFs for oxidative desulfurization: What matters?. *Green Chem.* **22**, 6351–6356 (2020).
73. Akbari, M., Nikoorazm, M., Tahmasbi, B. & Ghorbani-Choghamarani, A. Homoselective synthesis of tetrazoles and chemoselective oxidation of sulfides using Ni (II)-Schiff base complex stabilized on 3-dimensional mesoporous KIT-6 surface as a recyclable nanocatalyst. *Inorg. Chem. Commun.* **160**, 111852 (2024).
74. Emad-Abbas, N., Naji, J., Moradi, P. & Kikhavani, T. 3-(Sulfamic acid)-propyltriethoxysilane on biochar nanoparticles as a practical, biocompatible, recyclable and chemoselective nanocatalyst in organic reactions. *RSC Adv.* **14**, 22147–22158 (2024).
75. Rezaei, A., Ghorbani-Choghamarani, A. & Tahmasbi, B. Synthesis and characterization of nickel metal-organic framework including 4,6-diamino-2-mercaptopyrimidine and its catalytic application in organic reactions. *Catal. Lett.* **153**, 2005–2017 (2023).
76. Nikoorazm, M. et al. Synthesis of a new complex of lanthanum on MCM-41 as an efficient and reusable heterogeneous catalyst for the chemoselective synthesis of sulfoxides and tetrahydrobenzo[b]pyrans. *J. Porous Mater.* **31**, 511–526 (2024).
77. Jabbari, A., Nikoorazm, M. & Moradi, P. Two Schiff-base complexes of cadmium and manganese on modified MCM-41 as practical, recyclable and selective nanocatalysts for the synthesis of sulfoxides. *J. Porous Mater.* **30**, 1395–1402 (2023).
78. Jabbari, A., Nikoorazm, M. & Moradi, P. A V(O)-Schiff-base complex on MCM-41 as an efficient, reusable, and chemoselective nanocatalyst for the oxidative coupling of thiols and oxidation of sulfides. *Res. Chem. Intermed.* **49**, 1485–1505 (2023).

79. Yang, P., Lu, C., Hua, N. & Du, Y. Titanium dioxide nanoparticles co-doped with Fe3+ and Eu3+ ions for photocatalysis. *Mater. Lett.* **57**, 794–801 (2002).
80. Fan, Z. et al. Gd-modified MnOx for the selective catalytic reduction of NO by NH3: The promoting effect of Gd on the catalytic performance and sulfur resistance. *J. Chem. Eng.* **348**, 820–830 (2018).
81. Meng, D. et al. A highly effective catalyst of Sm-MnOx for the NH$_3$-SCR of NOx at low temperature: Promotional role of Sm and its catalytic performance. *ACS Catal.* **5**, 5973–5983 (2015).
82. Sun, P. et al. The enhanced performance of MnOx catalyst for NH3-SCR reaction by the modification with Eu Appl. *Catal. A General* **531**, 129–138 (2017).
83. Zhu, Y., Zhang, Y., Xiao, R., Huang, T. & Shen, K. Novel holmium-modified Fe-Mn/TiO$_2$ catalysts with a broad temperature window and high sulfur dioxide tolerance for low-temperature SCR. *Catal. Commun.* **88**, 64–67 (2017).
84. Caravan, P., Ellison, J. J., McMurry, T. J. & Lauffer, R. B. Gadolinium(III) chelates as MRI contrast agents: Structure, dynamics, and applications. *Chem. Rev.* **99**, 2293–2352 (1999).
85. Cheng, X. Q. et al. Structural, morphological, optical and photocatalytic properties of Gd-doped TiO$_2$ films. *Thin Solid Films* **615**, 13–18 (2016).
86. Lu, D. et al. Two-dimensional TiO$_2$-based nanosheets co-modified by surface-enriched carbon dots and Gd$_2$O$_3$ nanoparticles for efficient visible-light-driven photocatalysis. *Appl. Surf. Sci.* **396**, 185–201 (2017).
87. Phuruangrat, A., Cheed-Im, U., Thongtem, T. & Thongtem, S. Influence of Gd dopant on photocatalytic properties of MoO$_3$ nanobelts. *Mater. Lett.* **173**, 158–161 (2016).
88. Homaeigohar, S. The nanosized dye adsorbents for water treatment. *Nanomaterials* **10**, 295 (2020).
89. Sarkar, B., Goyal, R., Pendem, C., Sasaki, T. & Bal, R. Highly nanodispersed Gd-doped Ni/ZSM-5 catalyst for enhanced carbon-resistant dry reforming of methane. *J. Mol. Catal. A: Chem.* **424**, 17–26 (2016).
90. Mahmoud, H. R. Novel mesoporous Gd^{3+} doped Cr$_2$O$_3$ nanomaterials: Synthesis, characterization, catalytic and antitumor applications. *Adv. Powder Technol.* **27**, 1446–1452 (2016).
91. Mohammadi, M., Khodamorady, M., Tahmasbi, B., Bahrami, K. & Ghorbani-Choghamarani, A. Boehmite nanoparticles as versatile support for organic–inorganic hybrid materials: Synthesis, functionalization, and applications in eco-friendly catalysis. *J. Ind. Eng. Chem.* **97**, 1–78 (2021).
92. Ghorbani-Choghamarani, A., Aghavandi, H. & Mohammadi, M. Boehmite@ SiO2@ Tris (hydroxymethyl) aminomethane-Cu (I): a novel, highly efficient and reusable nanocatalyst for the C-C bond formation and the synthesis of 5-substituted 1H-tetrazoles in green media Appl. *Organomet. Chem.* **34**(10), e5804 (2020).
93. Jani, M. A. & Bahrami, K. Synthesis of 5-substituted 1H-tetrazoles and oxidation of sulfides by using boehmite nanoparticles/nickel-curcumin as a robust and extremely efficient green nanocatalyst. *Appl. Organomet. Chem.* **34**, e6014 (2020).
94. Jafari, F., Ghorbani-Choghamarani, A. & Hasanzadeh, N. Guanidine complex of copper supported on boehmite nanoparticles as practical, recyclable, chemo and homoselective organic–inorganic hybrid nanocatalyst for organic reactions. *Appl. Organomet. Chem.* **34**, e5901 (2020).
95. Moradi, P. & Ghorbani-Choghamarani, A. Efficient synthesis of 5-substituted tetrazoles catalysed by palladium–S-methylisothiourea complex supported on boehmite nanoparticles. *Appl. Organomet. Chem.* **31**, e3602 (2017).
96. Tahmasbi, B. & Ghorbani-Choghamarani, A. First report of the direct supporting of palladium–arginine complex on boehmite nanoparticles and application in the synthesis of 5-substituted tetrazoles. *Appl. Organomet. Chem.* **31**, e3644 (2017).
97. Jabbari, A., Tahmasbi, B., Nikoorazm, M. & Ghorbani-Choghamarani, A. A new Pd-Schiff-base complex on boehmite nanoparticles: Its application in Suzuki reaction and synthesis of tetrazoles. *Appl. Organomet. Chem.* **32**, e4295 (2018).
98. Tamoradi, T., Ghorbani-Choghamarani, A. & Ghadermazi, M. CoFe$_2$O$_4$@ glycine-M (M = Pr, Tb and Yb): Three green, novel, efficient and magnetically-recoverable nanocatalysts for synthesis of 5-substituted 1H-tetrazoles and oxidation of sulfides in green condition. *Solid State Sci.* **88**, 81–94 (2019).
99. Karimian, A., Namvar-Mhaboub, M. & Abbasi, R. Methionine-coated Fe$_3$O$_4$ nanoparticles: An efficient and reusable nanomagnetic catalyst for the synthesis of 5-substituted 1H-tetrazoles. *Russ. J. Org. Chem.* **56**, 1646–1653 (2020).
100. Fatahi, H., Jafarzadeh, M. & Pourmanouchehri, Z. Synthesis of α-aminonitriles and 5-substituted 1H-tetrazoles using an efficient nanocatalyst of Fe$_3$O$_4$@SiO$_2$–APTES-supported trifluoroacetic acid. *J. Heterocycl. Chem.* **56**, 2090–2098 (2019).
101. Moradi, P., Hajjami, M. & Tahmasbi, B. Fabricated copper catalyst on biochar nanoparticles for the synthesis of tetrazoles as antimicrobial agents. *Polyhedron* **175**, 114169 (2020).
102. Tamoradi, T., Ghorbani-Choghamarani, A., Ghadermazi, M. & Veisi, H. SBA-15@Glycine-M (M= Ni and Cu): Two green, novel and efficient catalysts for the one-pot synthesis of 5-substituted tetrazole and polyhydroquinoline derivatives. *Solid State Sci.* **91**, 96–107 (2019).
103. Ghafouri-Nejad, R. & Hajjami, M. Synthesis and characterization of Cu–N, N′-Dicyclohexylcarbodiimide supported on CMK-3 as a novel, efficient and recoverable nanocatalyst for synthesis of tetrazole, polyhydroquinoline, and sulfoxide derivatives. *React. Kinet. Mech. Catal.* **129**, 371–389 (2020).
104. Salahshournia, B., Hamadi, H. & Nobakht, V. Engineering a Cu-MOF nano-catalyst by using post-synthetic modification for the preparation of 5-substituted 1H-tetrazoles. *Appl. Organomet. Chem.* **32**, e4416 (2018).
105. Matloubi Moghaddam, F., Eslami, M. & Ghadirian, N. MCM-41-SO$_3$H as an efficient reusable nano-ordered heterogeneous catalyst for the synthesis of divers 1-000 5-substituted 1H-tetrazoles. *Sci. Iran* **26**, 1463–1473 (2019).
106. Nikoorazm, M., Ghorbani-Choghamarani, A., Ghobadi, M. & Massahi, S. As an efficient, stable and recyclable organometallic catalyst for C–C coupling reactions and synthesis of 5-substituted tetrazoles. *Appl. Organomet. Chem.* **31**, e3848 (2017).
107. Nikoorazm, M., Moradi, P. & Noori, N. L-cysteine complex of palladium onto mesoporous channels of MCM-41 as reusable, homoselective and organic–inorganic hybrid nanocatalyst for the synthesis of tetrazoles. *J. Porous Mater.* **27**, 1159–1169 (2020).
108. Nikoorazm, M., Tahmasbi, B., Gholami, S. & Moradi, P. Copper and nickel immobilized on cytosine@ MCM-41: As highly efficient, reusable and organic–inorganic hybrid nanocatalysts for the homoselective synthesis of tetrazoles and pyranopyrazoles. *Appl. Organomet. Chem.* **34**, e5919 (2020).
109. Mohammadi, M., Ghorbani-Choghamarani, A. & Ramish, S. M. [ZrFe$_2$O$_4$@ SiO$_2$-N-(TMSP)-ASP-Pd (0)] complex: Synthesis, characterizations, and its application as a nanomagnetic catalyst in cross-coupling and click reactions.. *J. Mol. Struct.* **1292**, 136115 (2023).
110. Norouzi, M., Noormoradi, N. & Mohammadi, M. Nanomagnetic tetraaza (N 4 donor) macrocyclic Schiff base complex of copper (ii): Synthesis, characterizations, and its catalytic application in click reactions. *Nanoscale Adv.* **5**, 6594–6605 (2023).
111. Akbarzadeh, P., Koukabi, N. & Kolvari, E. Anchoring of triethanolamine-Cu(II) complex on magnetic carbon nanotube as a promising recyclable catalyst for the synthesis of 5-substituted 1H-tetrazoles from aldehydes. *Mol. Diversity.* **24**, 319–333 (2020).
112. Kazemnejadi, M. et al. Copper coordinated-poly (α-amino acid) decorated on magnetite graphene oxide as an efficient heterogeneous magnetically recoverable catalyst for the selective synthesis of 5-and 1-substituted tetrazoles from various sources: A comparative study. *Appl. Organomet. Chem.* **34**, e5273 (2020).
113. Lakshmi Kantam, M., Kumar, K. B. S. & Sridhar, C. Nanocrystalline ZnO as an efficient heterogeneous catalyst for the synthesis of 5-substituted 1H-tetrazoles. *Adv. Synth. Catal.* **347**, 1212–1214 (2005).
114. Agawane, S. M. & Nagarkar, J. M. Synthesis of 5-substituted 1 H-tetrazoles using a nano ZnO/Co$_3$O$_4$ catalyst. *Sci. Technol.* **2**, 1324–1327 (2012).
115. Potdar, S. M., Bandivadekar, P. & Waghmode, K. T. Manganese(II) chloride tetrahydrate as an efficient catalyst for the preparation of 5-aryl-1H-tetrazoles via [3+2] cycloaddition of sodium azide and nitriles. *Org. Prep. Proced. Int.* **57**, 1–8 (2024).

116. Aydinli, E., Hameed, Z. A., Goksu, H. & Adem, S. Investigation of the efficacy on tyrosinase enzyme of 5-substituted-1H-tetrazole derivatives synthesized with Pd-containing nanoparticle. *Chem. Sci. J.* **136**, 22 (2024).

117. Nikoorazm, M. & Erfani, Z. Core–shell nanostructure (Fe_3O_4@MCM-41@Cu-P2C) as a highly efficient and recoverable nanocatalyst for the synthesis of polyhydroquinoline, 5-substituted 1H-tetrazoles and sulfides. *Chem. Phys. Lett.* **737**, 136784 (2019).

118. Moeini, N., Molaei, S. & Ghadermazi, M. Dysprosium (III) supported on $CoFe_2O_4$ MNPs as a heterogeneous catalyst for the selective oxidation of sulfides and synthesis of symmetrical disulfides. *J. Mol. Struct.* **1246**, 131071 (2021).

119. Davarpanah, J. & Kiasat, A. R. Synthesis and characterization of SBA-polyperoxyacid: An efficient heterogeneous solid peroxyacid catalyst for epoxidation of alkenes. *Catal. Comm.* **46**, 75–80 (2014).

120. Zhang, Z. et al. Fabrication of Au nanoparticles supported on $CoFe_2O_4$ nanotubes by polyaniline assisted self-assembly strategy and their magnetically recoverable catalytic properties. *Appl. Surf. Sci.* **363**, 578–585 (2016).

121. Ma, X. et al. Hydrogenation of dimethyl oxalate to ethylene glycol over mesoporous Cu-MCM-41 catalysts. *AIChE J.* **59**, 2530–2539 (2013).

122. Rajabi, F., Fayyaz, F. & Luque, R. Cytosine-functionalized SBA-15 mesoporous nanomaterials: Synthesis, characterization and catalytic applications. *Micropor. Mesopor. Mat.* **253**, 64–70 (2017).

123. Zare, M., Moradi-Shoeili, Z., Esmailpour, P., Akbayrak, S. & Özkar, S. Oxazine containing molybdenum(VI)–oxodiperoxo complex immobilized on SBA-15 as highly active and selective catalyst in the oxidation of alkenes to epoxides under solvent-free conditions. *Micropor. Mesopor. Mat.* **251**, 173–180 (2017).

124. Svidrytski, A., Hlushkou, D., Thommes, M., Monson, P. A. & Tallarek, U. Modeling the impact of mesoporous silica microstructures on the adsorption hysteresis loop. *J. Phys. Chem. C.* **124**, 21646–21655 (2020).

125. Yazdanpour, N. & Sharifnia, S. Photocatalytic conversion of greenhouse gases (CO_2 and CH_4) using copper phthalocyanine modified TiO_2. *Sol. Energy Mater. Sol. Cells.* **118**, 1–8 (2013).

126. Navaei, Z., Zanjanchi, M. A. & Appl, S. N. Synthesis of an efficient photocatalyst by incorporation of phthalocyanine into KIT-6. *SN Appl. Sci.* **2**, 1037 (2020).

127. Rath, D. & Parida, K. M. Copper and nickel modified MCM-41 an efficient catalyst for hydrodehalogenation of chlorobenzene at room temperature. *Ind. Eng. Chem. Res.* **50**, 2839–2849 (2011).

128. Gómez-Quero, S., Díaz, E., Cárdenas-Lizana, F. & Keane, M. A. Solvent effects in the catalytic hydrotreament of haloaromatics over Pd/Al_2O_3 in water+organic mixtures. *Chem. Eng. Sci.* **65**, 3786–3797 (2010).

129. Roy, S. K., Dutta, D. & Talukdar, A. K. Highly effective methylated Ti MCM-41 catalyst for cyclohexene oxidation. *Mater. Res. Bull.* **103**, 38–46 (2018).

130. Rama, V., Kanagaraj, K. & Pitchumani, K. Syntheses of 5-substituted 1H-tetrazoles catalyzed by reusable CoY zeolite. *J. Org. Chem.* **76**, 9090–9095 (2011).

131. Molaei, S., Tamoradi, T., Ghadermazi, M. & Ghorbani-Choghamarani, A. Synthesis and characterization of MCM-41@AMPD@Zn as a novel and recoverable mesostructured catalyst for oxidation of sulfur containing compounds and synthesis of 5-substituted tetrazoles. *Micropor. Mesopor. Mat.* **272**, 241–250 (2018).

132. Zamani, L., Mirjalili, B., Zomorodian, K. & Zomorodian, S. Synthesis and Characterization of 5-Substituted 1H-Tetrazoles in the Presence of Nano-TiCl4.SiO2. *South Afr. J. Chem. Suid-Afrikaanse tydskrif vir chemie.* **68**, 133–137 (2015).

133. Das, R. & Chakraborty, D. Cu (II)-catalyzed oxidation of sulfides. *Tetrahedron Lett.* **51**, 6255–6258 (2010).

134. Ghorbani-Choghamarani, A., Moradi, P. & Tahmasbi, B. Ni-SMTU@boehmite: As an efficient and recyclable nanocatalyst for oxidation reactions. *RSC Adv.* **6**, 56458–56466 (2016).

135. Jayaseeli, A. M. I. & Rajagopal, S. [Iron (III)–salen] ion catalyzed H_2O_2 oxidation of organic sulfides and sulfoxides. *J. Mol. Catal. Chem.* **309**, 103–110 (2009).

136. Jayaseeli, A. M. I., Ramdass, A. & Rajagopal, S. Selective H_2O_2 oxidation of organic sulfides to sulfoxides catalyzed by cobalt(III)–salen ion. *Polyhedron* **100**, 59–66 (2015).

137. Tamoradi, T., Ghorbani-Choghamarani, A. & Ghadermazi, M. Fe_3O_4–adenine–Zn: A novel, green, and magnetically recoverable catalyst for the synthesis of 5-substituted tetrazoles and oxidation of sulfur containing compounds. *New J Chem.* **41**, 11714–11721 (2017).

138. Tamoradi, T., Ghadermazi, M. & Ghorbani-Choghamarani, A. Ni(II)-Adenine complex coated Fe_3O_4 nanoparticles as high reusable nanocatalyst for the synthesis of polyhydroquinoline derivatives and oxidation reactions. *Appl. Organomet. Chem.* **32**, e3974 (2018).

139. Ghorbani-Choghamarani, A., Darvishnejad, Z. & Norouzi, M. Cu (II)-Schiff base complex-functionalized magnetic Fe3O4 nanoparticles: A heterogeneous catalyst for various oxidation reactions. *Appl. Organo Met. Chem.* **29**, 170–175 (2015).

140. Tamoradi, T., Ghorbani-Choghamarani, A. & Ghadermazi, M. Synthesis of new zirconium complex supported on MCM-41 and its application as an efficient catalyst for synthesis of sulfides and the oxidation of sulfur containing compounds. *Appl. Organo Met. Chem.* **32**(5), e4340 (2018).

141. Amani, K., Zolfigol, M. A., Ghorbani-Choghamarani, A. & Hajjami, M. Ferric nitrate in the presence of catalytic amounts of KBr or NaBr: an efficient and homoselective catalytic media for the selective oxidation of sulfides to sulfoxides. *Monatsh. Chem.* **140**, 65–68 (2009).

142. Chehardoli, G. & Zolfigol, M.A. *Phosphorus Sulfur Silicon Relat. Elem.* **185**, 193–203 (2009).

143. Hasaninejad, A., Chehardoli, G., Zolfigol, M. A. & Abdoli, A. Uronium hydrogen sulfate/urea-hydrogen peroxide as a green and metal-free catalytic system for the efficient, chemo-, and homoselective oxidation of sulfides to sulfoxides. *Phosphorus Sulfur Silicon Relat. Elem.* **186**, 271–280 (2011).

144. Zolfigol, M. A. et al. Chemo and homoselective catalytic oxidation of sulfides to sulfoxides with supported nitric acid on silica gel and poly vinyl pyrrolidine (PVP) catalyzed by KBr and/or NaBr. *Catal. Comm.* **9**, 1739–1744 (2008).

Acknowledgements

Author contributions

Somayeh Molaei contributed to the design and implementation of the research, the analysis of the results, the writing of the manuscript, and writing review and editing, Mohammad Ghadermazi contributed to conceptualization, methodology, validation, formal analysis, resources, supervision, project administration, and funding acquisition.

Declarations

Competing interests
The authors declare no competing interests.

Additional information
Supplementary Information The online version contains supplementary material available at https://doi.org/10.1038/s41598-025-97420-6.

Correspondence and requests for materials should be addressed to M.G.

Reprints and permissions information is available at www.nature.com/reprints.

Publisher's note Springer Nature remains neutral with regard to jurisdictional claims in published maps and institutional affiliations.